NUMERICAL CALCULATION OF VELOCITY, TEMPERATURE AND ENTROPY GENERATION IN THREE–DIMENSIONAL CHANNEL FLOWS WITH LONGITUDINAL VORTEX GENERATORS

A Thesis Submitted
in Partial Fulfilment of the Requirements
for the Degree of

MASTER OF TECHNOLOGY

by

SUDIPTA BISWAS

to the

DEPARTMENT OF MECHANICAL ENGINEERING
INDIAN INSTITUTE OF TECHNOLOGY KANPUR

JANUARY 1992

CERTIFICATE

This is to certify that the thesis entitled **''NUMERICAL CALCULATION OF VELOCITY, TEMPERATURE AND ENTROPY GENERATION IN THREE-DIMENSIONAL CHANNEL FLOWS WITH LONGITUDINAL VORTEX GENERATORS''** which is being submitted by Mr. Sudipta Biswas to the Mechanical Engineering Department of Indian Institute of Technology, Kanpur, in partial fulfilment for the award of Master of Technology is a record of bonafide work carried out by him in the Department of Mechanical Engineering, Indian Institute of Technology, Kanpur, under my supervision and guidance.

Gautam Biswas

(Dr Gautam Biswas)

Department of Mechanical Engineering

Indian Institute of Technology

Kanpur

ABSTRACT

The present study has been undertaken to determine numerically the flow structure and heat transfer characteristics in a rectangular channel with built-in vortex generators in the form of slender delta wing and winglet pair. Each wing or winglet pair induces streamwise longitudinal vortices behind them which cause a spiralling flow and entrain fluid from outside into the core of the vortices. Finally, these vortices disrupt the growth of thermal boundary layer and bring about the enhancement of heat transfer between the flowing fluid and the channel walls. The prediction of complex three dimensional flow structure and augmentation of heat transfer are made by making use of the solution of complete Navier-Stokes and energy equations. The geometrical configuration represents either an element of a compact gas-liquid fin-tube crossflow heat exchanger or an element of a plate-fin crossflow heat exchanger.

In practice the vortex generators can be mounted on the flat surfaces of the above mentioned heat exchangers by punching or embossing the flat surfaces. The effect of these punched holes, known as stamping, on heat transfer and skin friction characteristics has also been accounted. The effect of angle of attack of the wing generators, their geometrical shape and

Reynolds number on heat transfer enhancement and skin friction distribution have been obtained as well. It is found that the enhancement in heat transfer is more for the case with built-in vortex generators and without any stamping than for the case with punched holes beneath the vortex generators. Heat transfer coefficient is found to increase with increase in angle of attack. Finally, the delta wing shows a better performance in heat transfer enhancement as compared to winglet pair for the same geometrical area of the wing and the winglet pair.

However, most convective heat transfer processes encounter two types of losses, namely, losses due to fluid friction and those due to heat transfer across finite temperature gradient. These two phenomena are manifestation of thermodynamic irreversibility and an evaluation of the process from this standpoint is referred to as the second-law analysis. A second-law analysis is made for the above mentioned augmentation techniques and conclusions are drawn about the influence of type of vortex generators (wings / winglets) on irreversibility.

CONTENTS

NOMENCLATURE

B = channel width

Br = ratio of wing span to width of the channel (b/B)

b = wing span

C_f = skin friction, $\left[2\left(\frac{\partial u}{\partial y}\right)_w\right] \Big/ \left(\rho U_{av}^2\right)$

$\overline{C}_f$ = combined spanwise average friction coefficient equation (23)

C_p = specific heat of the fluid

Ec = Eckert number

H = channel height

h = heat transfer coefficient, $-k\left(\frac{\partial T}{\partial y}\right)_w \Big/ (T_w - T_b)$

I = rate of destruction of exergy in the channel

k = thermal conductivity of the fluid

M = merit function

Nu = local Nusselt number based on bulk temperature of the fluid

$\overline{Nu}$ = spanwise average Nusselt number

$\overline{Nu}_o$ = average Nusselt number for the entire channel

Ns = total rate of nondimensional entropy generation in the entire channel, equation (13)

Ns_g = rate of nondimensional entropy generation per unit volume, equation (12)

P = nondimensional pressure, $p/\rho U_{av}^2$

p = pressure

Pr = Prandtl number, $\mu C_p / k$

Q = total rate of heat transfer to the fluid

Q_a = total rate of exergy transfer corresponding to energy transfer Q

q = wall heat flux

Re = Reynolds number, $U_{av} H / \nu$

r = ratio of wall temperature to ambient temperature = $T_w / T_a = T_w / T_\infty$

$\dot{S}$ = total rate of entropy generation in the entire channel

$\dot{S}_g$ = rate of entropy generation per unit volume, equation (8)

T = temperature

T_a = ambient temperature

$\bar{T}_b$ = average bulk temperature for the entire channel

t = time

U = u/ U_{av}

u = axial component of velocity

V = v/ U_{av}

v = vertical component of velocity

W = w / U_{av}

w = spanwise component of velocity

X = x / H

x = axial dimension of coordinates

Y = y / H

y = vertical or normal dimension of coordinates

Z = z / H

z = spanwise dimension of coordinates

reek symbols

α = aspect ratio of the channel, B / H

Δ = divergence of velocity

δ_{ij} = Kronecker delta

μ = dynamic viscosity of the fluid

ν = kinematic viscosity of the fluid

σ = stress tensor

$\bar{\theta}_b$ = average nondimensional bulk temperature for the entire channel = $(\bar{T}_b - T_\infty) / (T_w - T_\infty)$

τ = nondimensional time

Λ = aspect ratio of the wing, b^2 / S

Subscripts

w	= wall
b	= bulk condition
av	= average
1	= bottom fin-plate
2	= top fin-plate
sa	= spanwise combination of top and bottom plate

LIST OF FIGURES

ACKNOWLEDGEMENT

I take this opportunity to express my deepest regards, whole-hearted gratitude and thanks to my respected teacher and thesis supervisor Dr. Gautam Biswas, Assistant Professor, Department of Mechanical Engineering, Indian Institute of Technology, Kanpur, without whose necessary guidance, constant inspiration and encouragement I could not dare to make this venture.

I shall be failing in my duty if I do not express sincere greatfulness and thanks to my friends and colleagues, Mr. Aniruddha Mukhopadhyay and Mr. Prasanta Deb for their ungrudging help and suggestions throughout my stay in I I T / K.

The author is indebted to all faculty members of Mechanical Engineering Department, in general, and Dr. T. Sundararajan and Dr. V. Eswaran in particular, for their valuable advice and encouragement.

Finally, the author appreciates the help and inspiration he received from his family members and well wishers.

Sudipta Biswas
20/01/92
(Sudipta Biswas)

I. I. T. Kanpur

January, 1992

CHAPTER I

INTRODUCTION

Longitudinal vortices embedded in shear flows occur in many flow situations and have remarkable influence in design and development of heat exchangers. Heat exchangers are used extensively in the energy industry, the petrochemical industry, the process industry and the food industry. Improvement in heat exchanger design would have a direct impact on material saving, space saving and efficient use of energy. Figures 1(a) and 1(b) show typical arrangements of two different heat exchanger cores. It has been seen that the heat transfer coefficients on the flat surfaces of the above mentioned heat exchangers are significantly low. Augmentation of heat transfer is of special interest in these types of channel flows where the heat transfer between the fluid and the channel walls deteriorates as the boundary layer grows on the channel walls and the flow tends to become fully developed.

In order to disrupt the growth of thermal boundary layer and, thereby, increase heat transfer between the gas and the fin in the case of gas-liquid fin-tube crossflow heat exchanger and between the flowing fluid and the plates in the case of plate-fin

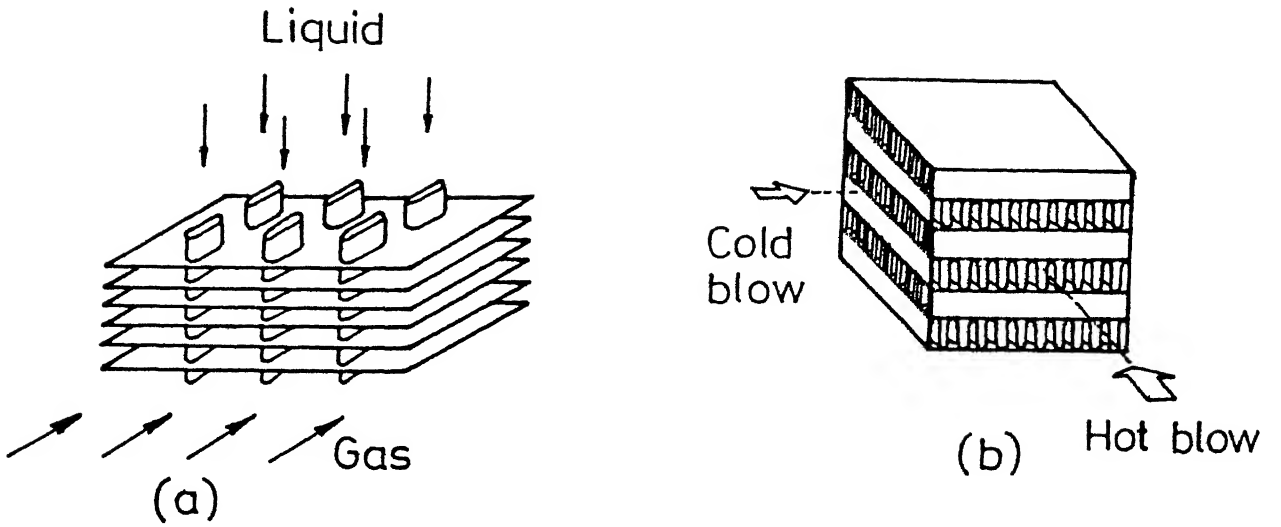

Fig 1 Typical arrangement of heat exchanger cores
(a) Gas-liquid fin-tube cross flow
(b) Plate-fin (single or multi pass)

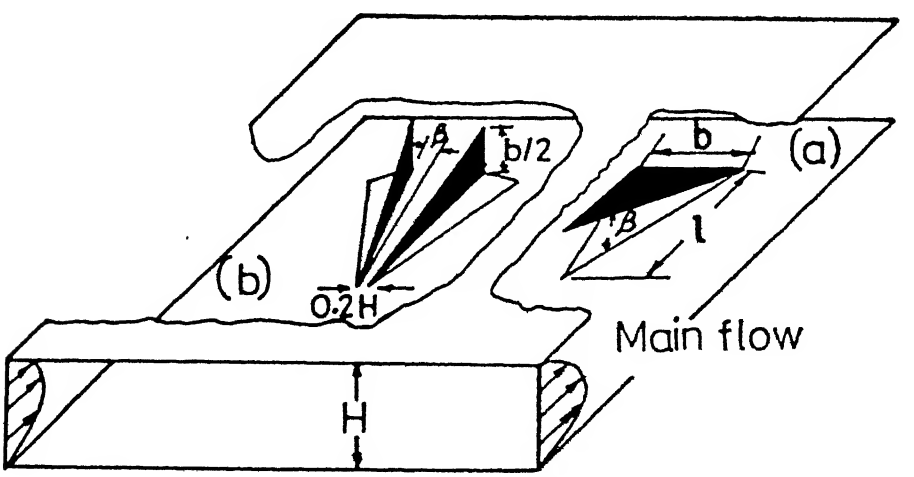

Fig. 2 Protrusions in the form of (a) delta wing and (b) winglet pair on the flat surface to enhance heat transfer.

heat exchangers Protrusions could be mounted on the flat surfaces. The protrusions in the form of slender wing-type vortex generators [Fig. 2 (a) and (b)] can bring about the desired augmentation of heat transfer at the expense of relatively less increase in pressure drop. These wing generators will take fluid from the underside of the wake and swirl it around the upper side entraining fluid from the channel-wall-region to the vortex-core-region. This mechanism finally culminates in the disruption of the growth of thermal boundary layer and consequent increase in heat transfer coefficient. Because of favourable pressure gradient in the channel, the longitudinal vortices will be stable and their effect will be perceived over an area which is many times the size of the wing generators. From the consideration of manufacturing, these vortex generators can easily be fabricated by cutting delta shape on the plates and then pushing them up. Finally, the slender wing generators can also act as spacers for the plate fins. Typically, the Reynolds numbers for such applications lie below 3000. Experimental investigations by Edwards and Alker [1], Russel, Jones and Lee [2] and Fiebig et al [3] and computational analysis by Fiebig et al [4] and Biswas et al [5] show that the vortex generators in the form of slender delta wings and winglet pairs are indeed very effective in augmentation of heat transfer. Velocity field and heat transfer

measurements were reported for slender wings embedded in a turbulent boundary layer (see Elbeck and Eaton [6]; Ligrani et al [7]). Recently, a computational study has been performed by Biswas and Chattopadhyay [8] for laminar flows in a geometrical configuration of delta wing placed inside a channel. They have discussed about the influence of angle of attack and Reynolds number on heat transfer and skin friction coefficients. Fiebig et al [9] have shown that the delta wings are more effective than the winglet pairs with regard to augmentation of heat transfer coefficient on a flat surface. It has also been shown that the drag generated in the channel due to winglet pair is considerably less than that due to the wing. In this investigation we shall try to compare the performance of wings and winglets by taking into consideration both the parameters, namely, the augmentation of heat transfer and the associated flow losses.

The aforesaid comparison may be accomplished with the help of second-law analysis. The inherent irreversibility associated with any convective heat transfer process results in penalty to useful power. Estimation of irreversibilities of a process from the entropy generation rate and the minimization of the same by a suitable adjustment of the governing input parameters is usually referred to as second-law or thermodynamic optimization of the process. In such analyses, the

irreversibilities due to external interaction of energy and internal dissipative effects are simultaneously taken care of.

The present work provides a qualitative and quantitative performance data for delta wing and winglet pair in a channel for different operating conditions. Solution of complete Navier-Stokes and energy equations and a detailed analysis of flow structure provide deep insight into the mechanistic modelling of the complicated flow configuration. Finally, a numerical evaluation of entropy generation in the heat transfer process for the proposed model is presented. Based on an evaluation of irreversibility, this study draws some conclusions about the influence of type of vortex generators (wings / winglets) on efficient use of energy.

CHAPTER II

LITERATURE SURVEY

The objectives of the present study has been briefly outlined in the previous chapter. The present chapter deals with a survey of relevant literature in the field of augmentation of heat transfer by surface mounted obstacles. The survey helps in suggesting further works that should be carried out to accomplish the objectives enumerated earlier.

In both gas-liquid fin-tube crossflow heat-exchangers and plate-fin heat exchangers (single or multi-pass), the heat transfer coefficient between the flowing fluid and the flat plates are very low. In order to improve the heat transfer performance of the heat exchangers, protrusions could be mounted on the flat surfaces. Of course, the heat transfer enhancement with the help of obstacles is always accompanied by a corresponding rise in pressure drop. It has been observed, however, that the protrusions in the form of slender delta wing or winglet pair can augment heat transfer significantly at the expense of relatively less increase in pressure penalty. The enhancement is obtained due to the generation of streamwise longitudinal vortices behind the protrusions and consequent better mixing of hot and cold fluid in the downstream. The slender wings and winglets are streamline

bodies, hence the associated pressure drop is also less. Van Dyke [10] has illustrated the flow visualization results of the vortices formed by delta wing and slender bodies. One of the flow visualization is reproduced in fig.2(c).

The first experimental result regarding augmentation of heat transfer by vortex generators has been reported by Edwards and Alkar [1]. They, however, used bluff bodies (cubes) as vortex generators. Russel, Jones and Lee [2] has presented some quantitative results for heat transfer and pressure loss due to small aspect ratio winglets. They have compared square winglets with delta wings and found, in contrary to the results of other investigators, a better performance for the winglets.

Experimental investigations due to Fiebig, Kallweit, and Mitra [3] is the first systematic study to compare the performance of different kinds of vortex generators in the reynolds number range of 1360 to 2270. Their observations have established the fact that the delta wing is the best vortex generator from heat transfer point of view. Another important feature of their observations is that the heat transfer coefficient increases with increase in angle of attack. They have also pointed out that the ratio of highest heat transfer enhancement to the friction factor increment is achieved with delta wing at a small angle of attack, about 10°. Their flow visualization by Laser technique has

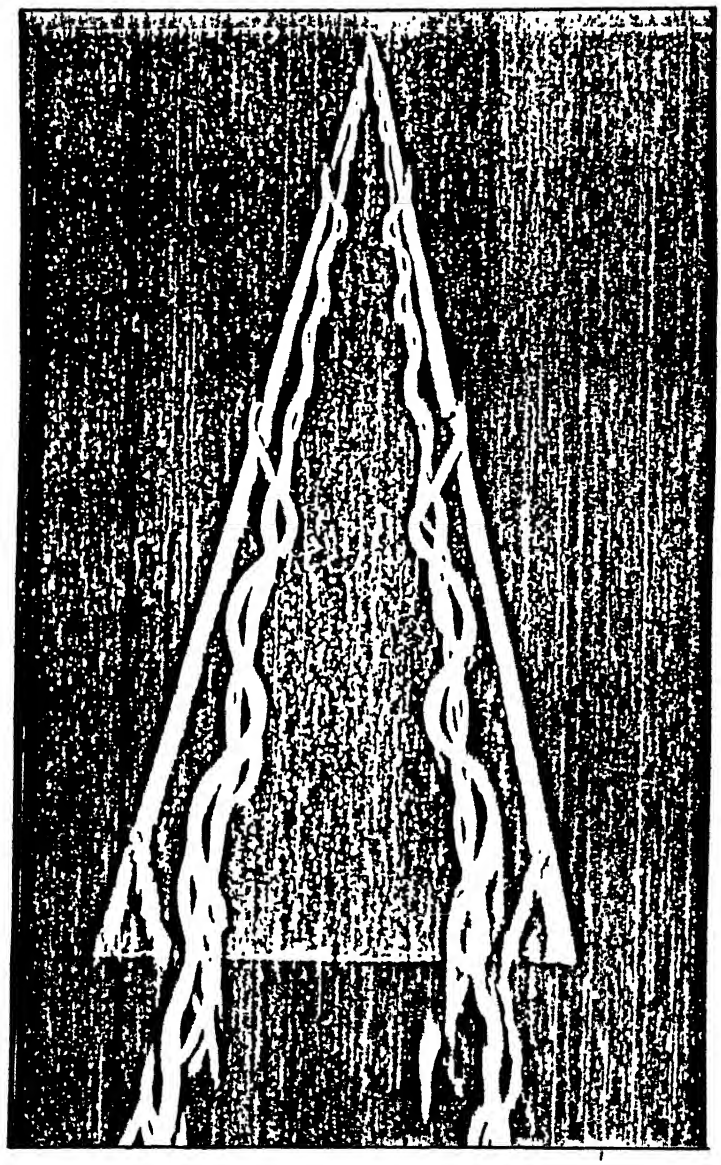

Fig. 2(c) Plan view of vortices formed by a slender delta wing.
courtesy of H. Werlé, ONERA, France

revealed that the concentrated vortex pair generated by a small aspect ratio delta wing at large angle of attack has elliptic shape due to the influence of channel walls. High aspect ratio delta wings have shown a turbulent structure in the vortex core.

Formation of streamwise longitudinal vortices behind a slender aerodynamic object is a research topic of considerable interest for several years. Both the theoretical and experimental investigations on flow past a delta wing have been conducted and reported in literature by a number of researchers. Among them Winter [11], Fink [12], Mardsen et al [13], Peckham [14], Earnshaw et al [15] and Lawford [16] are noteworthy.

Experimental measurements by Winter was followed by the very early nonlinear theory of rectangular wings of Bollay [17]. More realistic representation of the physics of vortex formation has been furnished by Brown et al [18], Mangler et al [19] and smith et al [20]. Use of thin aerofoil theory provides good approximation of the the strength of the leading edge vortices and the lift. Of course, in trailing edge part, their results show some discrepancy with experiments. Rehbach [21] and Kandil et al [22] have obtained better results with non-conical theory. Computational solution of non-conical flow field and pressure distribution on wing surface has also been attempted by Rubbert and co-workers [23,24]. Their study suffers from some numerical

complications in the vicinity of trailing edge.

Hummel [25] has made important contribution in revealing the complex flow structure behind a delta wing. He conducted experiments and presented pressure distribution, vortex structure etc of the flow around a delta wing of unit aspect ratio with an angle of attack of 20°.

Many researchers have observed longitudinal vortices in various complex flow configurations. Naturally, the interaction of such vortices with boundary layer and its effect on heat transfer was a subject of interest to them. Some examples are Taylor-Gortler vortices in boundary layers on concave curved surfaces, horseshoe vortices formed by an obstruction protruding from a surface and wingtip vortices impinging on a downstream surface. The embedded vortex is capable of strongly perturbing the boundary layer thickness and influencing the heat transfer characteristics. In addition, longitudinal vortices usually maintain their coherence over a long streamwise distance. As a consequence, the heat transfer effects behind a vortex generator are very persistent. Eibeck and Eaton [6], , Westphal and Mehta [26] worked extensively in this field with more focus to the turbulent layer.

Eibeck and Eaton [6] conducted experiment on longitudinal vortices embedded in a turbulent boundary layer and

resultant heat transfer effects. Longitudinal vortices are found to influence significantly the heat transfer behaviour. Local Stanton number increased as great as 24 percent resulting in a net increase in spanwise average heat transfer coefficient. Despite the presence of turbulent diffusion, the influence of longitudinal vortices on momentum and energy transport could be traced at a location as far downstream as 60 wing chords behind the delta wing.

In the last decade researchers attempted to explore the aforesaid problems using numerical schemes. Brockmeier et al [27] have computed the flow in a channel with built-in wing type vortex generator where full Navier-Stokes equations were solved.

Thomas et al [28] have computed low-speed laminar flow over a low aspect ratio delta wing upto 40° angle of attack using an upwind biased finite volume algorithm. The differencing scheme used are second-order accurate and a multigrid algorithm is employed to promote convergence to steady state. The predicted results and lift coefficient of the wing have remarkable agreement with experiments due to Hummel [25] and others. At 40° angle of attack, a bubble-type vortex breakdown is evident in the computations.

Biswas et al [5] have attempted to compute laminar mixed convection in a rectangular duct with built-in delta wing

using a modified version of MAC (Marker and Cell) algorithm. A number of computations have been performed with and without free convection for different values of Re, Gr (Grashof number) and angle of attack. Enhancement of heat transfer between the gas and the channel walls is evidenced. The augmentation is mainly due to longitudinal vortices generated by the wing. Buoyancy induced secondary flow increases the vortex strength and improves the heat transfer still further.

Westphal and Mehta [26] have studied the effect of oscillating vortex on a turbulent boundary layer. The meander is simulated by forcing a periodic lateral translation of a half-delta wing vortex generator at a low frequency of 1 Hz and one half amplitude of 0.5 cm. The effect of the meander is found to flatten the vorticity contours at the stations where they are originally round. The Reynolds stresses are also found to be significantly affected.

The disturbance to the growth of thermal boundary layer can also be accomplished by using a multi-louvered plate-fin surface. Investigations by Achaichia a Cowell [28] provides a detailed performance data for louvered fin surfaces. However, by using louvered fins, enhancement is obtained at the price of high pressure drop.

The study of irreversibility in convective heat transfer

has become an important topic from the standpoint of effective utilization of energy. It has been shown by Bejan ([29], [30], [31]) that the irreversibility brought about by any heat transfer process results in penalty to useful power. In such analyses, the irreversibilities due to external interaction of energy and internal dissipative effects are simultaneously taken care of. Estimation of irreversibilities of a process from the entropy production rate and the minimization of the same by a suitable adjustment of the governing input parameters is usually referred to as second-law or thermodynamic optimization of the process. Among the related works involving thermodynamic optimization, the analyses of heat transfer in cryogenic apparatus (Bejan and Smith, [32]), study of counter-flow heat exchangers (Sarangi and Chowdhury, [33]) and swirling flow through a cylindrical duct (Mukherjee, Biswas and Nag, [34]) are a few. The objective of the present article is to evaluate numerically the entropy generation of heat transfer processes in a rectangular duct involving augmentation by generating streamwise longitudinal vortices. Based on an evaluation of irreversibility, this study draws some conclusions about the influence of type of vortex generators (wings / winglets) on efficient use of energy.

CHAPTER III

STATEMENT OF THE PROBLEM

Computation is performed in a channel which is formed by two neighboring fins (Fig.3). An obstacle in the form of a delta-wing or winglet pair (of zero thickness) is placed inside it. The base of the wing is fixed on the bottom wall and the apex faces the incoming flow stream with an angle of attack. In the case of winglet pair, one side is fixed on the bottom wall and the trailing edge is free for each winglet. Since symmetry prevails in the vertical central plane of the channel, the flow field in only half of the channel has to be computed. The dimensionless equations for continuity, momentum and energy may be expressed in the following conservative forms as

$$\Delta = \frac{\partial U}{\partial X} + \frac{\partial V}{\partial Y} + \frac{\partial W}{\partial Z} = 0 \qquad (1)$$

$$\frac{\partial U}{\partial \tau} + \frac{\partial U^2}{\partial X} + \frac{\partial UV}{\partial Y} + \frac{\partial UW}{\partial Z} = - \frac{\partial P}{\partial X} + \frac{\nabla^2 U}{Re} \qquad (2)$$

$$\frac{\partial V}{\partial \tau} + \frac{\partial UV}{\partial X} + \frac{\partial V^2}{\partial Y} + \frac{\partial VW}{\partial Z} = - \frac{\partial P}{\partial Y} + \frac{\nabla^2 V}{Re} \qquad (3)$$

$$\frac{\partial W}{\partial \tau} + \frac{\partial UW}{\partial X} + \frac{\partial VW}{\partial Y} + \frac{\partial W^2}{\partial Z} = - \frac{\partial P}{\partial Z} + \frac{\nabla^2 W}{Re} \qquad (4)$$

$$\frac{\partial \theta}{\partial \tau} + \frac{\partial U\theta}{\partial X} + \frac{\partial V\theta}{\partial Y} + \frac{\partial W\theta}{\partial Z} = \frac{\nabla^2 \theta}{Re.Pr} \qquad (5)$$

In the above equations, velocities have been nondimensionalized with the average incoming velocity U_{av} at the channel inlet, all lengths with the channel height H, the pressure

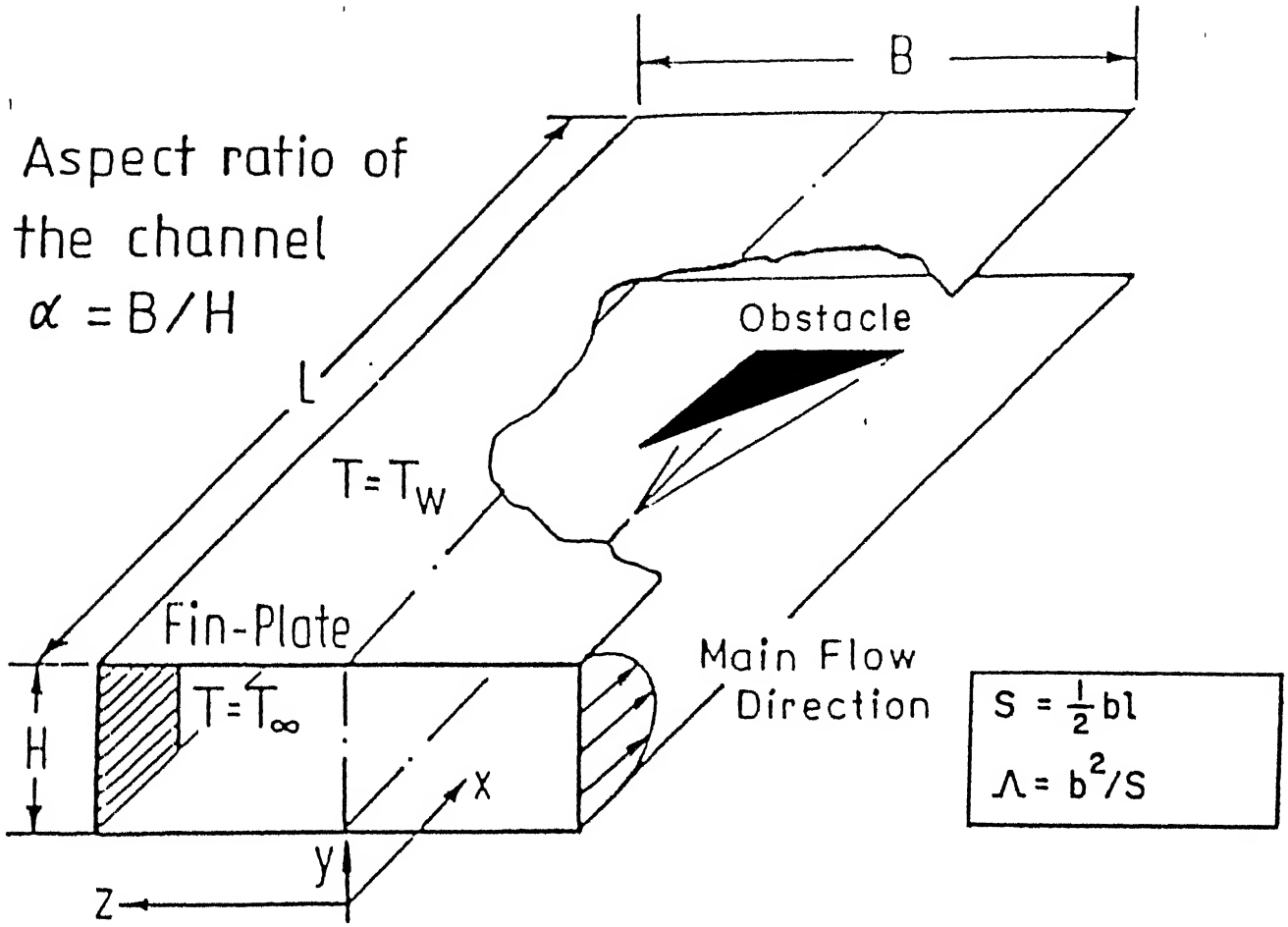

Type of obstacle (protrusion)

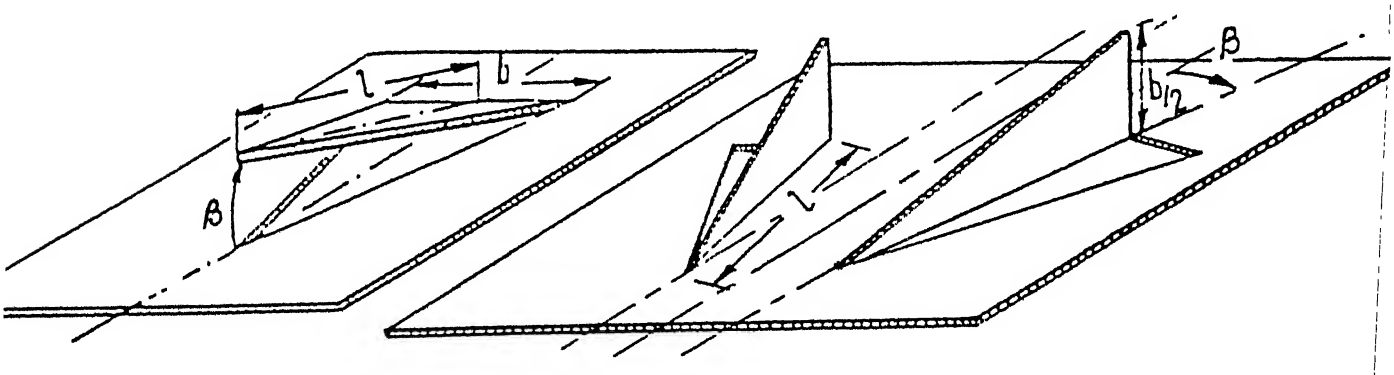

Delta wing Winglet pair

Fig.3 Flow model for computation

with ρU_{av}^2 and the nondimensional temperature is defined as $\theta = (T - T_\infty) / (T_w - T_\infty)$. Boundary conditions of interest in this investigation are

Top and bottom surfaces :

$$u = v = w = 0 \; ; \quad T = T_w$$

Side wall ($z = B / 2$) and mid plane ($z = 0$) :

$$w = (\partial v/\partial z) = (\partial u/\partial z) = (\partial T/\partial z) = 0$$

At the channel inlet :

$$u = u(y) \; , \; v = w = 0 \; , \quad T = T_\infty$$

At the exit, the boundary conditions for the dependent variables are obtained by setting the second derivatives of them in the flow direction equal to zero in order to ensure a smooth transition through the outflow boundary :

$$\frac{\partial^2 u}{\partial x^2} = \frac{\partial^2 v}{\partial x^2} = \frac{\partial^2 w}{\partial x^2} = \frac{\partial^2 T}{\partial x^2} = 0$$

No-slip boundary conditions for the velocities on the obstacles are used. The temperature of the obstacle is constant and equal to T_w.

While computing the case with stamping under the vortex generators, we have used periodic boundary conditions to take care of the holes due to punching on the flat plates. The period length for these periodic boundary conditions is equal to the channel height H [Fig.4(e)]. However, the boundary conditions for the fictitious cells on the bottom are :

$$u_{i,1,k} = u_{i,JRE,k}$$

$$v_{i,1,k} = 0.5 \left(v_{i,JRE,k} + v_{i,1,k} \right)$$

$$w_{i,1,k} = w_{i,JRE,k}$$

$$p_{i,1,k} = p_{i,JRE,k}$$

and on the top :

$$u_{i,JIM,k} = u_{i,2,k}$$

$$v_{i,JIM,k} = v_{i,2,k}$$

$$v_{i,JRE,k} = 0.5 \left(v_{i,1,k} + v_{i,JRE,k} \right)$$

$$w_{i,JIM,k} = w_{i,2,k}$$

$$p_{i,JIM,k} = p_{i,2,k}$$

The above two sets of boundary conditions are applied to all (i, k) locations on the hole. Such boundary conditions have also been discussed by Hirt, Nichols and Romero [35]

Nusselt Number

In order to have a quantitative distinction of the heat transfer performance the combined spanwise average Nusselt number

$$\overline{Nu}_{sa} = \frac{B \left[q_1 + q_2 \right]}{2\int_0^{B/2} \left[T_{w1}(x,z) - T_b(x) \right] dz + 2\int_0^{B/2} \left[T_{w2}(x,z) - T_b(x) \right] dz} \cdot \frac{H}{K} \qquad (6)$$

has been calculated at each longitudinal location to depict heat transfer at any axial position in the channel. The solution of energy equation provides with temperature value at each cell in the channel. The velocity quantities are known beforehand from the

solution of Navier-Stokes equations. These values are plugged in equation (6) to evaluate the combined spanwise average Nusselt number at each longitudinal section in the channel.

The average Nusselt number for the entire channel is calculated as

$$\overline{Nu}_c = \frac{1}{L} \int_0^L \overline{Nu}_{ea} dx \qquad (7)$$

Entropy Generation

The rate of entropy generation per unit volume is given by Kirkwood and Crawford [36] and Bird et al [37] as :

$$\dot{S}_a = - \frac{1}{T^2} (q \cdot \nabla T) - \frac{1}{T} (\sigma : \nabla \bar{V}) \qquad (8)$$

The first term on the right-hand side of (8) may be written as :

$$- \frac{1}{T^2} (q \cdot \nabla T) = \frac{k}{T^2} \left[\left(\frac{\partial T}{\partial x} \right)^2 + \left(\frac{\partial T}{\partial y} \right)^2 + \left(\frac{\partial T}{\partial z} \right)^2 \right] \qquad (9)$$

The second term on the right-hand side of equation (8) is expanded as

$$(\sigma : \nabla \bar{V}) = \left(p + \frac{2}{3} \mu \Delta \right) \delta_{ij} \left(\frac{\partial u_i}{\partial x_j} \right) - \mu \left(\frac{\partial u_i}{\partial x_j} + \frac{\partial u_j}{\partial x_i} \right) \frac{\partial u_i}{\partial x_j}$$

or, $$(\sigma : \nabla \bar{V}) = \left(p + \frac{2}{3} \mu \Delta \right) \Delta - \mu \left[2 \frac{\partial u}{\partial x} \frac{\partial u}{\partial x} + \left(\frac{\partial u}{\partial y} + \frac{\partial v}{\partial x} \right) \frac{\partial u}{\partial y} \right.$$

$$+ \left(\frac{\partial u}{\partial z} + \frac{\partial w}{\partial x} \right) \frac{\partial u}{\partial z} + \left(\frac{\partial v}{\partial x} + \frac{\partial u}{\partial y} \right) \frac{\partial v}{\partial x} + 2 \frac{\partial v}{\partial y} \frac{\partial v}{\partial y} + \left(\frac{\partial v}{\partial z} + \frac{\partial w}{\partial y} \right) \frac{\partial v}{\partial z}$$

$$\left. + \left(\frac{\partial w}{\partial x} + \frac{\partial u}{\partial z} \right) \frac{\partial w}{\partial x} + \left(\frac{\partial w}{\partial y} + \frac{\partial v}{\partial z} \right) \frac{\partial w}{\partial y} + 2 \frac{\partial w}{\partial z} \frac{\partial w}{\partial z} \right] \qquad (10)$$

After invoking incompressibility condition [equation (1)], equation (10) can be written as :

$$- \frac{\sigma : \nabla \bar{V}}{T} = \frac{\mu}{T} \left[2 \left\{ \left(\frac{\partial u}{\partial x} \right)^2 + \left(\frac{\partial v}{\partial y} \right)^2 + \left(\frac{\partial w}{\partial z} \right)^2 \right\} \right.$$

$$\left. \left(\frac{\partial u}{\partial y} + \frac{\partial v}{\partial x} \right)^2 + \left(\frac{\partial v}{\partial z} + \frac{\partial w}{\partial y} \right)^2 + \left(\frac{\partial u}{\partial z} + \frac{\partial w}{\partial x} \right)^2 \right] \qquad (11)$$

Use of equations (9) and (11) in equation (8) and nondimensionalization yields :

$$Ns_s = \frac{\dot{S}_s H^2}{k}$$

$$= \frac{(r-1)^2}{[\theta (r-1) + 1]^2} \cdot \left[\left(\frac{\partial \theta}{\partial X} \right)^2 + \left(\frac{\partial \theta}{\partial Y} \right)^2 + \left(\frac{\partial \theta}{\partial Z} \right)^2 \right]$$

$$+ \frac{Ec \cdot Pr}{[\theta (r-1) + 1]} \cdot \left[2 \left\{ \left(\frac{\partial U}{\partial X} \right)^2 + \left(\frac{\partial V}{\partial Y} \right)^2 + \left(\frac{\partial W}{\partial Z} \right)^2 \right\} \right.$$

$$\left. + \left(\frac{\partial U}{\partial Y} + \frac{\partial V}{\partial X} \right)^2 + \left(\frac{\partial U}{\partial Z} + \frac{\partial W}{\partial X} \right)^2 + \left(\frac{\partial V}{\partial Z} + \frac{\partial W}{\partial Y} \right)^2 \right] \qquad (12)$$

As expected, the irreversibility indicator Ns_s contains two additive parts, one due to conduction in the presence of non-zero temperature gradient, and the other accounting for

viscous dissipation of mechanical power throughout the flow. However, if the velocity and temperature fields are completely known, we can find out the values of nondimensional entropy generation per unit volume (Ns_g) at each cell of the flow domain. After evaluating this quantity, we integrate Ns_g over the entire volume to get nondimensional volumetric entropy generation in the channel as :

$$Ns = \iiint Ns_g \, dX \, dY \, dZ \qquad (13)$$

Merit Function

From this analysis, it is possible to evaluate the rate of energy transferred usefully as well as destruction of exergy due irreversibilities.

If Q is the total rate of heat transfer, then

$$Q = \bar{h}_c \left(T_w - \bar{T}_b \right) \cdot 2 B L$$

or,
$$Q = 4 \, \overline{Nu}_c \, k \, L \left(T_w - \bar{T}_b \right) \qquad (14)$$

In equation (14), a channel of aspect ratio = 2 has been considered, i.e., $B / H = 2$.

The equation (14) can be written as :

$$Q = 4 \, k \, L \, \overline{Nu}_c \, T_w \left(1 - \frac{1}{r} \right) \cdot \left(\theta_w - \bar{\theta}_b \right) \qquad (15)$$

The rate of exergy transfer accompanying energy transfer at a rate of Q is given by Moran [38] as

$$Q_a = Q \left[1 - \frac{T_a}{T_w} \right]$$

$$= Q \left[1 - \frac{1}{r} \right] \qquad (16)$$

where T_a, the exergy reference environment temperature has been considered as the ambient temperature T_∞. The wall temperature T_w has been considered as a suitable temperature at the surface where heat transfer takes place. If $\dot{S}$ is the total rate of entropy generation, the destruction of exergy is

$$I = T_a \cdot \dot{S}$$

or, $$I = \frac{T_\infty}{T_w} T_w \dot{S} \qquad [\text{ following the argument } T_a = T_\infty]$$

or, $$I = \frac{1}{r} \cdot T_w \dot{S} \qquad (17)$$

As such, the total rate of entropy generation, $\dot{S}$, may be written as :

$$\dot{S} = \iiint \dot{S}_g \, dx \, dy \, dz$$

or, $$\dot{S} = \frac{k}{H^2} \iiint Ns_g \, d(HX) \, d(HY) \, d(HZ) \qquad (18)$$

Invoking equation (13) in equation (18), we obtain

$$\dot{S} = H \, k \, Ns \qquad (19)$$

Finally, equation (17) and equation (19) will yield

$$I = \frac{1}{r} T_v H k Ns \qquad (20)$$

A merit function is defined as the ratio of exergy transferred to the sum of exergy transferred and exergy destroyed.

or, $$M = \frac{Q_a}{Q_a + I} \qquad (21)$$

Substituting for Q_a from equation (15) and I from equation (21), we obtain,

$$M = \frac{4 (r-1)^2 \overline{Nu}_c (\theta_w - \bar{\theta}_b)}{4 (r-1)^2 \overline{Nu}_c (\theta_w - \bar{\theta}_b) + \frac{r H}{L} Ns} \qquad (22)$$

This merit function is now evaluated for various flow parameters in a channel using delta wing or winglet pairs as vortex generators. The merit of the merit function lies in its simultaneous accountability of exergy transferred and its destruction caused by irreversibilities associated with exergy transport and momentum transport. Irreversibilities due to external interaction and internal dissipative effects are together taken care of by this parameter. However, it might be observed that equation (22) is another form of second-law efficiency (Moran, [38]).

CHAPTER IV

METHOD OF SOLUTION

The nondimensional continuity, momentum and energy equations in conservative forms, written in terms of primitive variables [equations (1) - (5)], are solved by using a modified version of Marker and Cell (MAC) algorithm. The original version of MAC due to Harlow and Welch [39] was modified by Hirt and Cook [40]. In the original MAC method, the pressure field was obtained by directly solving the Poisson's equation for pressure, whereas, in modified MAC version, pressure values are calculated implicitly from continuity equation by a pressure-velocity iteration process. A related technique developed by Chorin [41] involved a simultaneous iteration on pressure and velocity components. Viecelli [42] has shown that the two methods as applied to the MAC algorithm are equivalent.

The computational domain is divided into a number of rectangular cells of edge length δX, δY and δZ along the X, Y and Z directions respectively. Cells are denoted by an index (i,j,k) implying the cell number as counted from the origin in X, Y and Z directions respectively. Staggered grid arrangement is used in which the velocity components are defined at the centre of the cell faces to which they are normal [Fig. 4(a)]. The pressure and temperature are defined at the centre of the cell.

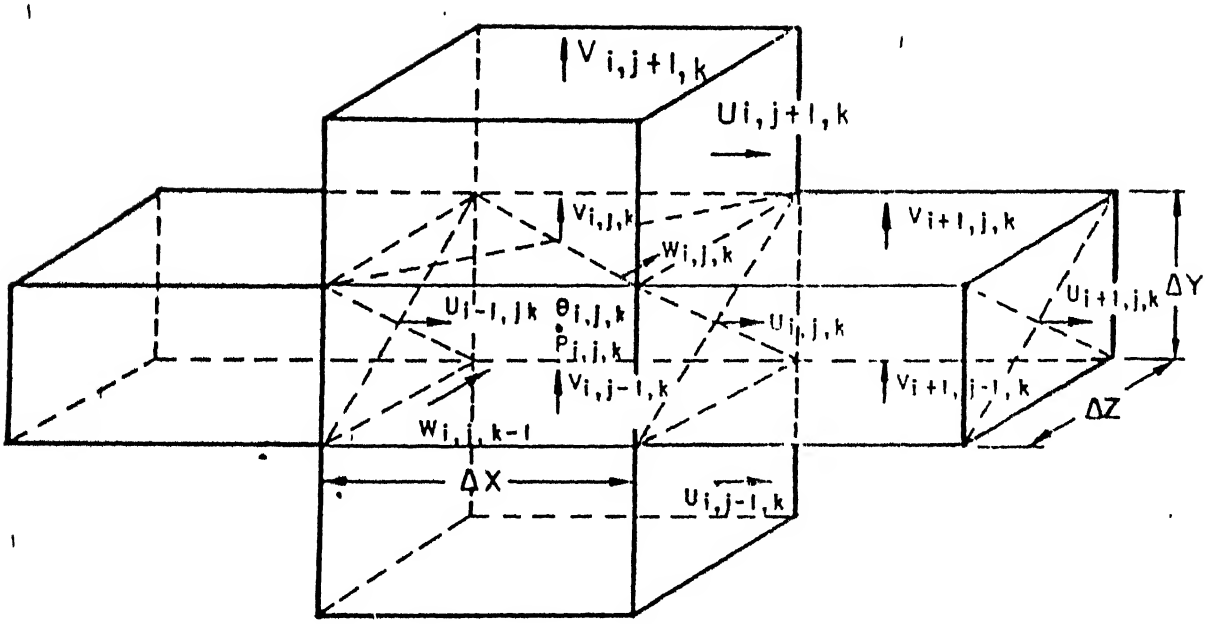

Fig. 4(a) Three dimentional staggered grid showing the locations of the discretized variables.

4.1 Computational Scheme

MAC is a semi-implicit scheme of solving complete unsteady Navier-Stokes equations where the advancement of velocity components with respect to time are obtained explicitly by calculating accelerations due to convection, diffusion and pressure gradient. After obtaining a provisional velocity field , for a particular time step, the continuity equation is solved implicitly. Hence MAC is an implicit-explicit scheme.

The complete Navier-Stokes equations are elliptic in space and parabolic in time. Hence their solution has to be time-marching. Again, since the equations are elliptic in space, we need boundary conditions on all confining boundaries — even at the outlet. To start the computation, a guess field of velocity, pressure and temperature are assumed. To compute compressible flow, a certain density field has also to be assumed ; and in that case, we have to solve another equation, namely, the equation of state. However, in our case, the flow-field is incompressible and we use constant density assumption.

From the guessed velocity and pressure fields, the corrected velocity and pressure fields are obtained by pressure-velocity iteration through continuity equation. Convergence of this iteration process ensures a divergence-free velocity field for the initial time-step. Now, this corrected pressure-velocity

field is used to calculate the velocity field for the next time step by making use of Navier-Stokes equations. The advancement of the velocities for one time step $\delta\tau$ is calculated by evaluating the accelerations caused by advection, diffusion and pressure gradient. The choice of the time increment value $\delta\tau$ is governed by stability criterion as discussed in section 4.4. However, this explicit time advancement may not lead to a velocity field with zero mass divergence in each cell. In the subsequent second stage, adjustments are done to ensure mass conservation in each cell. This is performed by manipulating the pressures as well as velocities in each cell through an iterative process, which, as mentioned earlier, is equivalent to solution of Poisson's equation for pressure. Details of pressure-velocity iteration procedure is discussed in section 4.3. The corrected pressure and velocity are now used to evaluate velocities for the next time step through the momentum equations. Thus the solution advances in time direction until the values of velocity components in between two consecutive time steps become identical implying steady state converged solution.

The solution of the energy equation is, however, relatively simple. After the steady converged velocity field is obtained, the velocity components are invoked in the energy equation making it linear in nature. The solution of the

temperature field is then obtained by a Successive Over Relaxation (SOR) technique.

4.2 Discretization and Numerical Boundary Conditions

The continuity equation is discretized by a simple first order differencing in such a way that the mass conservation is maintained. For a particular cell, mass divergence (for incompressible flow) is given by :

$$\Delta_{i,j,k} = \left(U_{i,j,k} - U_{i-1,j,k} \right) / \delta X + \left(V_{i,j,k} - V_{i,j-1,k} \right) / \delta Y + \left(W_{i,j,k} - W_{i,j,k-1} \right) / \delta Z$$

The convective terms of Navier-Stokes and energy equations are discretized by a hybrid scheme which combines upwind and central differencing to achieve the stability of upwind and formal accuracy of the central differencing (Spalding [43]). The discretization of one of the convective terms is shown below :

$$\frac{\partial (UV)}{\partial Y} = \frac{1}{4\,\delta Y} \Big[\left(V_{i,j,k} + V_{i+1,j,k} \right)\left(U_{i,j,k} + U_{i,j+1,k} \right) + \alpha \left(V_{i,j,k} + V_{i+1,j,k} \right)\left(U_{i,j,k} - U_{i,j+1,k} \right) - \left(V_{i,j-1,k} + V_{i+1,j-1,k} \right)\left(U_{i,j-1,k} + U_{i,j,k} \right) - \alpha \left(V_{i,j-1,k} - V_{i+1,j-1,k} \right)\left(U_{i,j-1,k} - U_{i,j,k} \right) \Big]$$

Here α is a weighing factor. When α is zero, the above

discretization will become a simple central differencing and when $\alpha = 1$, this is exactly the second upwind differencing. The choice of this factor α is also dictated by stability criterion as discussed in 4.4.

Discretization of temporal terms in equations (2) to (5) is done by simple forward differencing. All the second order terms are discretized by central difference. For example,

$$\frac{\partial U}{\partial \tau} = \left(U^{n+1}_{i,j,k} - U^{n}_{i,j,k} \right) / \delta\tau$$

$$\frac{\partial^2 U}{\partial X^2} = \frac{1}{(\delta X)^2} \left(U_{i+1,j,k} - 2U_{i,j,k} + U_{i-1,j,k} \right)$$

An important aspect of solving differential equations is the application of proper boundary conditions. Correct implementation of boundary conditions in the solution code requires special treatment. For prescribing velocities on the boundaries of the computational domain, four kinds of velocity boundary conditions are needed, namely, rigid-wall or no-slip boundary condition, symmetric or free-slip boundary condition, inflow boundary condition and outflow boundary condition. At any boundary, one velocity component will be normal and the other two will be tangential to the boundary. The normal velocity is easy to prescribe when the boundary coincides with a cell edge.

At the inlet, the axial velocity component is given the desired input value or a well defined profile. The vertical and spanwise velocity components at the inlet are assigned zero value. For the treatment of the no- slip and free-slip boundaries, we need to consider a layer of fictitious cells just outside the computational domain. On an no- slip wall, normal velocity components are directly set to zero, whereas, the tangential components on the wall are made zero by assigning the tangential velocities of the fictitious cells the same magnitude as those of the adjacent real cells but opposite sign. On a free-slip surface, the normal velocity is again zero, but here the tangential components in the fictitious cells have same magnitude and sign as those for the cells just inside the computational domain. For outflow boundary there is no unique prescription, but the general idea is to choose the boundary condition in such a way that it has minimum upstream influence. For this purpose, a useful approach is to set the second derivatives of the velocities equal to zero. This seems to keep the flow going smoothly out of the boundary.

For temperature boundary condition also, we have to make use of the imaginary cells. The temperature in the imaginary cells are set equal to the temperature values in the corresponding cells just inside the fluid region when a free-slip wall is concerned.

They are equal to ($2T_w - T_{i,j,k}$) in case of a conducting wall and for the assumption of a linear variation of temperature. However, a nonlinear temperature variation on the solid wall has been used in the present code, given by

$$T1 = TW5 - F112 \times T1(I,J,K) + F32 \times T1(I,J,K)$$

where, $TW5 = 5\ T_w$

$F112 = 11 / 2$

$F32 = 3 / 2$

At the inlet, uniform temperature profile has been employed. At the exit, the second derivative of the temperature in the axial direction is made equal to zero in order to ensure a smooth transition.

There are special modules to take care of the boundary conditions on the wing generator. Subroutines BCO, BCOV and BCOT implement the velocity and temperature boundary conditions on the vortex generator. BCO is the subroutine where the geometrical parameters of the vortex generator are taken care of. From Fig.4(b) and 4(c), the angle of attack of the vortex generator can be expressed as $\beta = \tan^{-1}(\delta Y/\delta X)$, aspect ratio $\Lambda = 2b / \ell$ where $b / 2 = (KC - KB).\delta Z$ and $\ell = (IB - IA).\delta X / \cos\beta$. Fig.4(b) further reveals that the U and V components of velocity fall directly on the surface of the obstacle and, therefore, are set equal to zero. Implementation of no-slip condition for U component

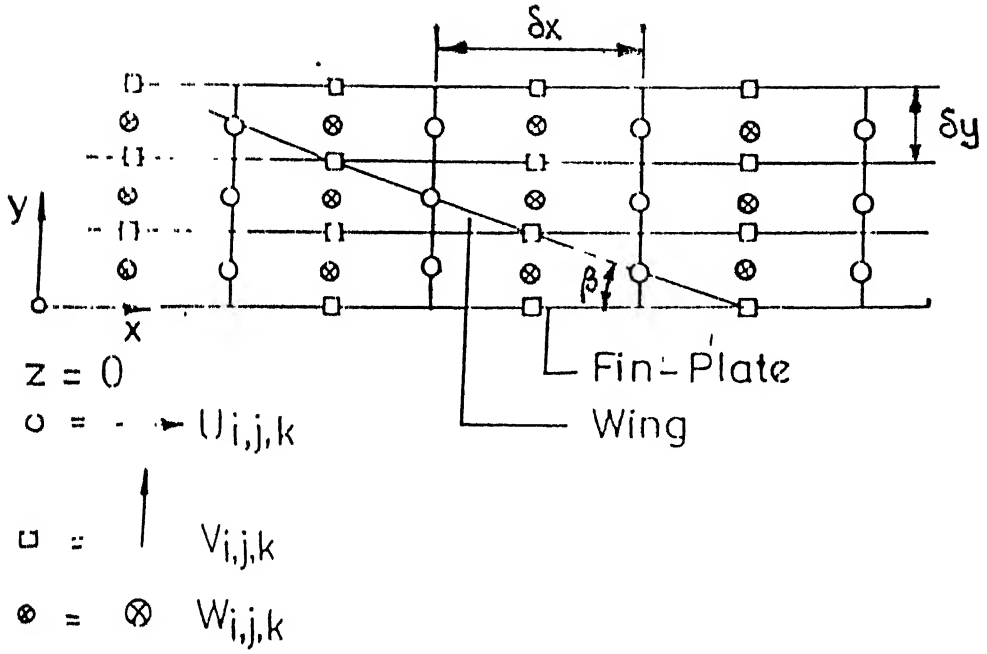

Fig. 4(b) Relative location of velocity components and wing on x-y plane at Z=0

velocity at the edge of the obstacle needs some manipulations which are incorporated in subroutine BCOV. From Fig.4(e), it is found that $U_{i,j,k+1/2} = 0$, or, in other words,

$$U_{i,j,k} = - U_{i,j,k+1}.$$

The W component of boundary also needs manipulation for its zero value on the surface of the obstacle. From Fig.4(e),

$$W_{i,j,k} = - W_{i,j-1,k}$$

$$W_{i,j,k} = - W_{i-1,j,k}$$

$$W_{i,j-1,k} = - W_{i,j,k}$$

$$W_{i-1,j,k} = - W_{i,j,k}$$

The temperature boundary conditions on the obstacle are taken care of in the subroutine BCOT and are diagramatically shown in Fig.4(d). The nondimensional temperature θ has been denoted in the code by T. The obstacle boundary conditions for temperature are :

$$T_{i,j,k} = 2T_w - T_{i-1,j,k}$$

$$T_{i,j,k} = 2T_w - T_{i,j-1,k}$$

$$T_{i-1,j+1,k} = 2T_w - T_{i-1,j,k}$$

$$T_{i-1,j+1,k} = 2T_w - T_{i-2,j+1,k} \quad \text{etc.}$$

4.3 Pressure-Velocity Iteration

Direct solution of Poisson's equation for pressure suffers from the inherent problem of prescribing pressure boundary

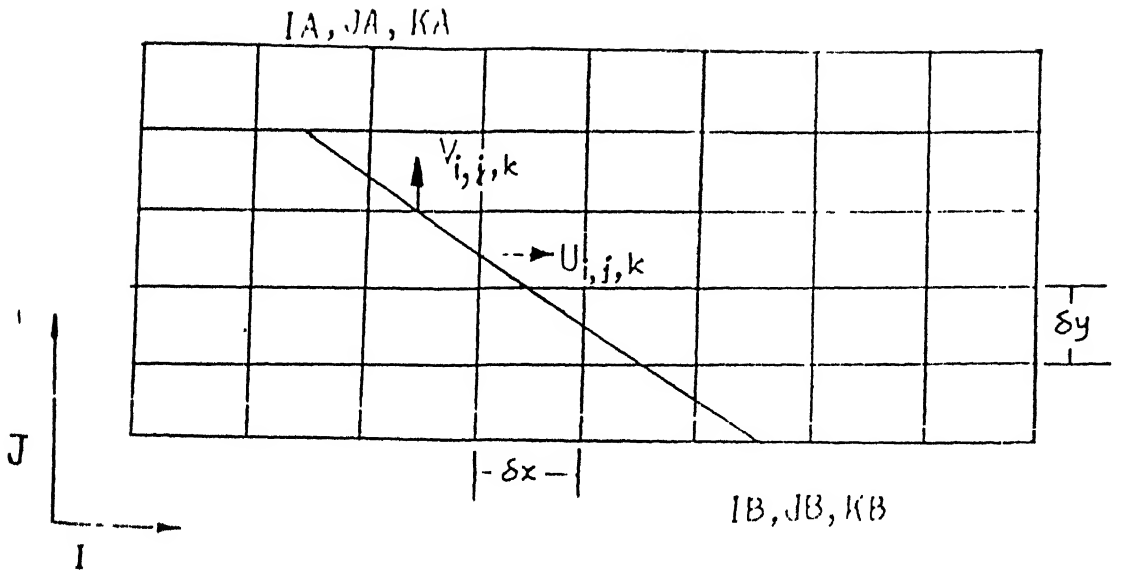

Fig.4(c) Relative location of the wing and the velocity components on i-j plane

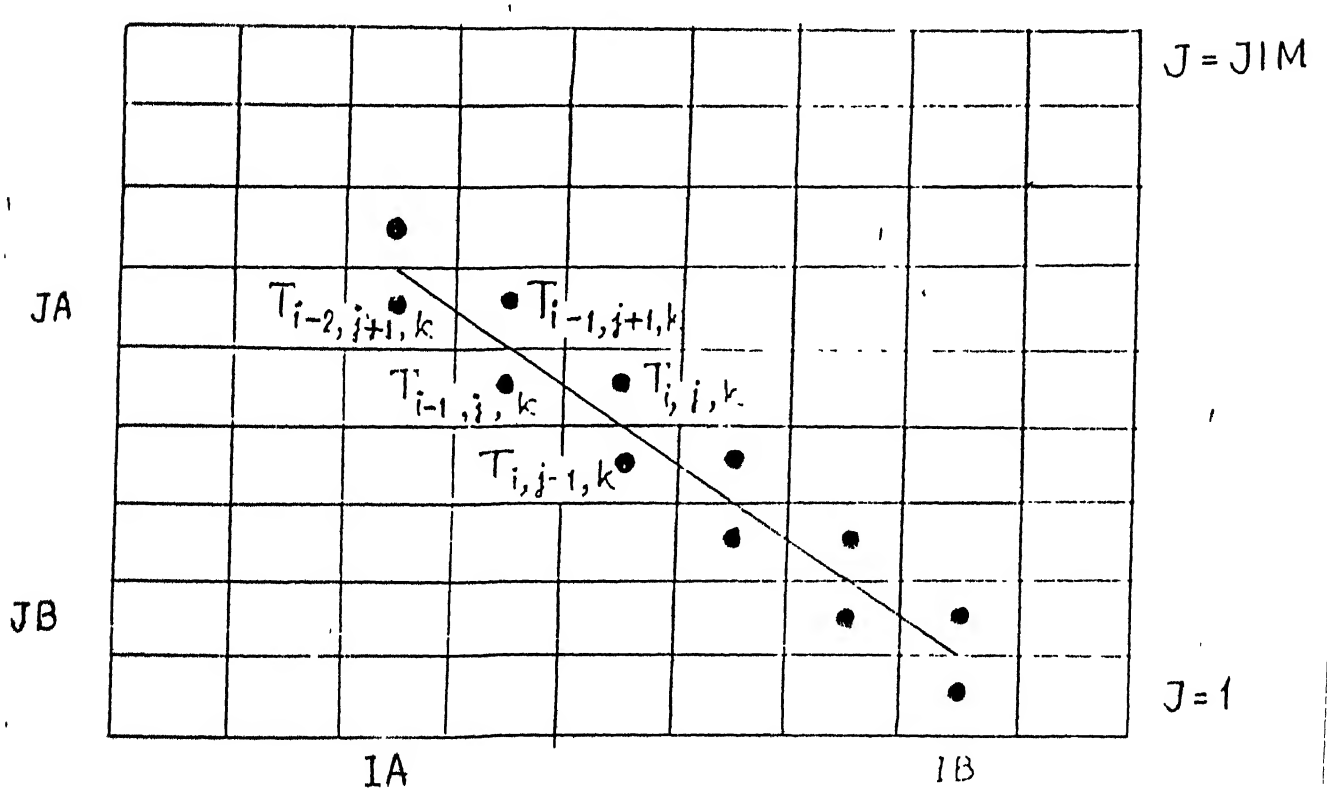

Fig.4(d) Thermal boundary conditions on the obstacle

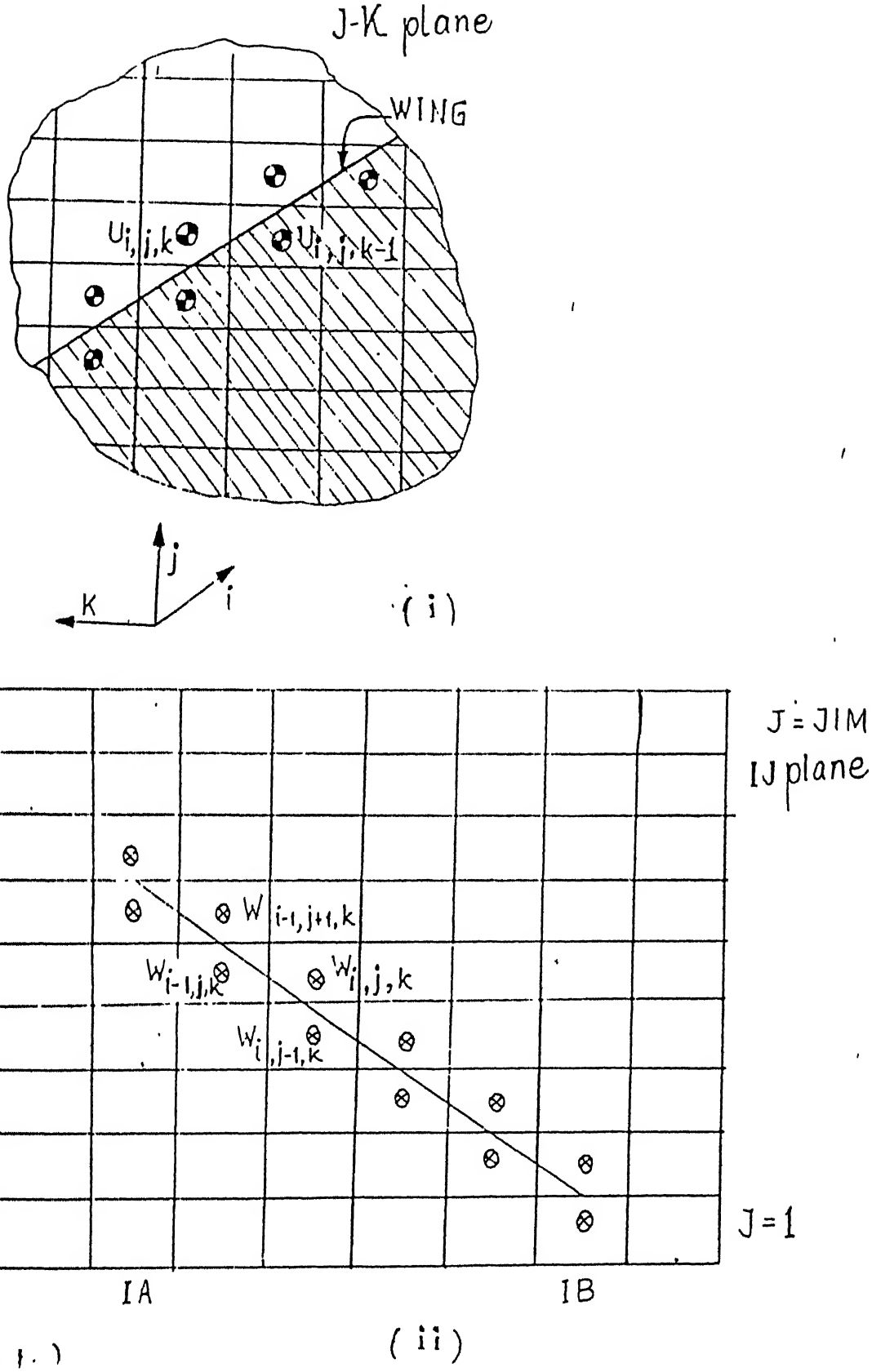

Fig. 4(e) Velocity boundary conditions on the obstade

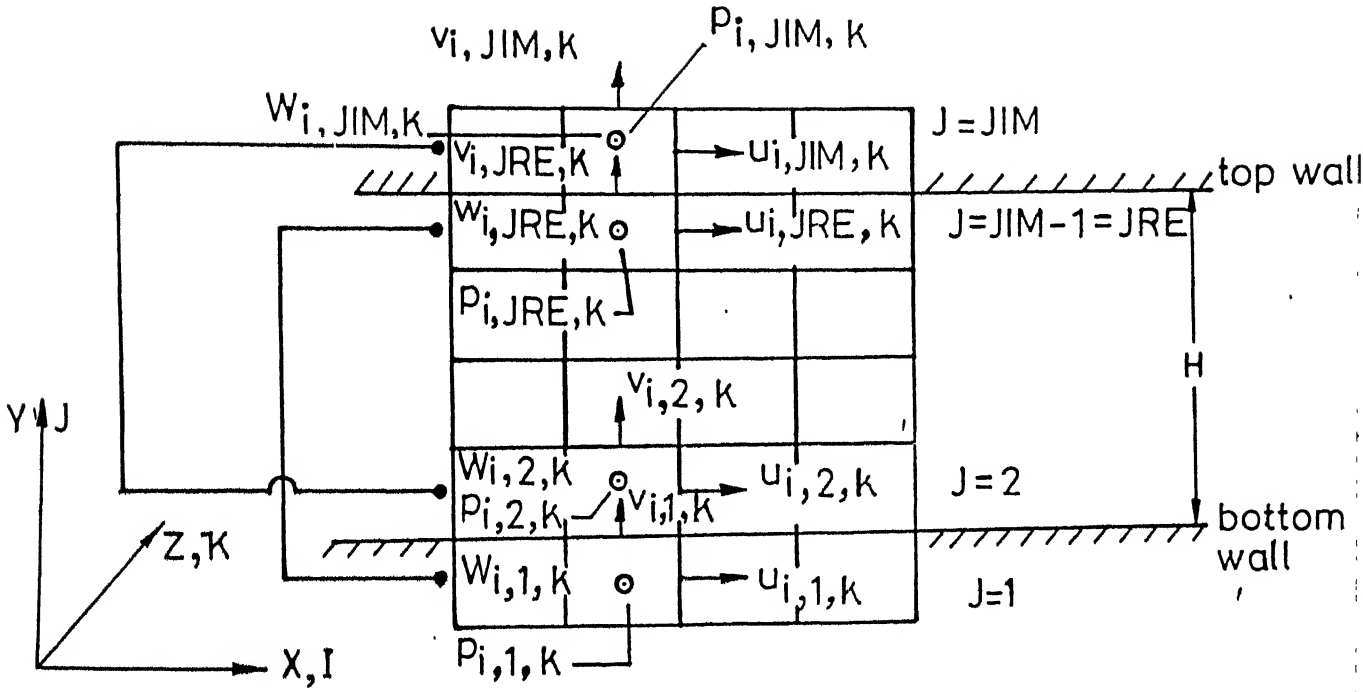

Fig. 4f Periodic boundary conditions for pressure and velocities on the top and the bottom wall

conditions. In this respect, the modified MAC algorithm due to Hirt and Cook [40] has a considerable edge over the original MAC method. The mathematically methodology of the iteration process is described herein :

If the velocity and pressure field are known at any time step, we can evaluate the velocity field for the next time step by explicitly calculating the accelerations due to advection, diffusion and pressure gradients through Navier-Stokes equations. As has been mentioned before, the explicitly advanced provisional velocities may not necessarily lead to a flow field with zero mass divergence in each cell, which means, at this stage the pressure distribution is not correct. Pressure in each cell will be corrected in such a way that there is no accumulation or annihilation of mass in the cell. The relationship between the explicitly advanced velocity component [at (n+1)-th time step] and the velocity at the previous time step [i.e. n-th time step] may be written as

$$\tilde{U}^{n+1}_{i,j,k} = U^{n}_{i,j,k} + \frac{\delta\tau \left(P^{n}_{i,j,k} - P^{n}_{i+1,j,k} \right)}{\delta X} + \delta\tau \left[\text{RESIDU} \right]^{n}_{i,j,k} \qquad (23)$$

where $\left[\text{RESIDU} \right]^{n}_{i,j,k}$ is the value of $\left[-\frac{\partial U^2}{\partial X} - \frac{\partial UV}{\partial Y} - \frac{\partial UW}{\partial Z} + \frac{\nabla^2 U}{Re} \right]$ at the (i,j,k) cell evaluated with the velocity values at the

n-th time step.

On the other hand, the corrected velocity component (unknown) will be related to the correct pressure (also unknown) in the following way :

$$U_{i,j,k}^{n+1} = U_{i,j,k}^{n} + \frac{\delta\tau\left(P_{i,j,k}^{n+1} - P_{i+1,j,k}^{n+1} \right)}{\delta X} + \delta\tau \left[\text{RESIDU} \right]_{i,j,k}^{n} \qquad (24)$$

From equations (23) and (24), one can write

$$U_{i,j,k}^{n+1} - \tilde{U}_{i,j,k}^{n+1} = \frac{\delta\tau\left(P'_{i,j,k} - P'_{i+1,j,k} \right)}{\delta X} = - \frac{\delta\tau\ \delta P'}{\delta X}$$

where $P'_{i,j,k} = P_{i,j,k}^{n+1} - P_{i,j,k}^{n}$

So, $U_{i,j,k}^{n+1} = \tilde{U}_{i,j,k}^{n+1} + \frac{\delta\tau\ \delta P'_{i,j,k}}{\delta X}$

Neither $\delta P'_{i,j,k}$ nor $U_{i,j,k}^{n+1}$ are known explicitly at this stage so that one can be calculated with the help of the other. Calculations are done in an iterative cycle and we write

$$U_{i,j,k}^{n+1} \longrightarrow \tilde{U}_{i,j,k}^{n+1} + \frac{\delta\tau\ \delta P'_{i,j,k}}{\delta X}$$

In the similar way we can complete the following array

$$
\left.
\begin{aligned}
U^{n+1}_{i,j,k} &\longrightarrow \tilde{U}^{n+1}_{i,j,k} + \frac{\delta\tau\ \delta P'_{i,j,k}}{\delta X} \\
U^{n+1}_{i-1,j,k} &\longrightarrow \tilde{U}^{n+1}_{i,j,k} - \frac{\delta\tau\ \delta P'_{i,j,k}}{\delta X} \\
V^{n+1}_{i,j,k} &\longrightarrow \tilde{V}^{n+1}_{i,j,k} + \frac{\delta\tau\ \delta P'_{i,j,k}}{\delta Y} \\
V^{n+1}_{i,j-1,k} &\longrightarrow \tilde{V}^{n+1}_{i,j,k} - \frac{\delta\tau\ \delta P'_{i,j,k}}{\delta Y} \\
W^{n+1}_{i,j,k} &\longrightarrow \tilde{W}^{n+1}_{i,j,k} + \frac{\delta\tau\ \delta P'_{i,j,k}}{\delta Z} \\
W^{n+1}_{i,j,k-1} &\longrightarrow \tilde{W}^{n+1}_{i,j,k} - \frac{\delta\tau\ \delta P'_{i,j,k}}{\delta Z}
\end{aligned}
\right\} \quad \ldots(25)
$$

The correction is done through 'continuity equation.

Plugging in the relationship (25) into continuity equation,

$$
\left[\frac{U^{n+1}_{i,j,k} - U^{n+1}_{i-1,j,k}}{\delta X} + \frac{V^{n+1}_{i,j,k} - V^{n+1}_{i,j-1,k}}{\delta Y} + \frac{W^{n+1}_{i,j,k} - W^{n+1}_{i,j,k-1}}{\delta Z} \right]
$$

$$
= \left[\frac{\tilde{U}^{n+1}_{i,j,k} - \tilde{U}^{n+1}_{i-1,j,k}}{\delta X} + \frac{\tilde{V}^{n+1}_{i,j,k} - \tilde{V}^{n+1}_{i,j-1,k}}{\delta Y} + \frac{\tilde{W}^{n+1}_{i,j,k} - \tilde{W}^{n+1}_{i,j,k-1}}{\delta Z} \right]
$$

$$
+ \frac{2\ \delta\tau\ \delta P'}{\delta X^2} + \frac{2\ \delta\tau\ \delta P'}{\delta Y^2} + \frac{2\ \delta\tau\ \delta P'}{\delta Z^2}
$$

$$
\text{or,} \quad 0 = \Delta_{i,j,k} + \delta P' \left[2\ \delta\tau \left(\frac{1}{\delta X^2} + \frac{1}{\delta Y^2} + \frac{1}{\delta Z^2} \right) \right]
$$

$$
\text{or,} \quad \delta P' = -\omega_o (\Delta_{i,j,k}) \Big/ \left[2\ \delta\tau \left(\frac{1}{\delta X^2} + \frac{1}{\delta Y^2} + \frac{1}{\delta Z^2} \right) \right] \qquad (26)
$$

where ω_o is an over relaxation factor which is introduced to accelerate the pressure correction process. Usually a value of $\omega_o = 1.7$ is used. After calculating $\delta P'$, velocities in each cell are corrected according to the equation set (25) and pressure in each cell is adjusted as

$$P_{i,j,k}^{n+1} \longrightarrow P_{i,j,k}^{n+1} + \delta P' \qquad (27)$$

This process is continued until the velocity divergence in each cell vanishes. If the velocity boundary conditions are correct and a divergence-free converged velocity field is obtained, eventually correct pressure will be evolved in all the cells including the cells on the boundary. This feature of Modified MAC method has been discussed in more details by Peyret and Taylor [44]. However, it was also shown by Brandt, Dendy and Ruppel [45] that the aforesaid pressure-velocity iteration procedure is equivalent to solution of Poisson's equation for pressure.

4.4 Numerical Stability

The rectangular cell sides δx, δY and δZ are related to the input parameters like angle of attack, wing aspect ratio, channel aspect ratio etc. Given the geometrical parameters of the flow model, δX δY and δZ can be obtained. Once the mesh has been chosen, the choice of time increment $\delta\tau$ is dictated by stability

criteria which are governed by two restrictions. The first restriction is known as Courant-Friedrichs-Lewy (CFL) condition which says that material can not move more than one cell in one time step. The difference equations assume fluxes only between adjacent cells. Mathematically, therefore, we should have

$$\delta\tau \leq \min \left[(\delta X / |U|), (\delta Y / |V|), (\delta Z / |W|) \right] \qquad (28)$$

where the minimum is with respect to every cell in the flow-domain. Typically $\delta\tau$ is chosen equal to one-third to two-third of the minimum cell transient time.

The second restriction is governed by grid-Fourier-number which states that the momentum must not diffuse through more than one cell in one time step. A linear stability analysis shows that this limitation implies

$$\nu\, \delta\tau \leq \frac{1}{2} \frac{\delta x^2\, \delta y^2\, \delta z^2}{(\delta x^2 + \delta y^2 + \delta z^2)}$$

In nondimensional terms this gives

$$\delta\tau \leq \frac{1}{2} \frac{\delta X^2\, \delta Y^2\, \delta Z^2}{(\delta X^2 + \delta Y^2 + \delta Z^2)} \cdot Re$$

Finally, $\delta\tau$ is chosen such that it satisfies the above two inequalities.

It has already been pointed out that the term α in the discretization of convective terms of equations (1) - (5) is an weighing factor which gives the desired amount of upstream (donor cell) differencing. $\alpha = 0$ gives space centred differencing and α

= 1 gives full upstream or donor cell form, which is stable provided the fluid is not permitted to cross more than one cell in one time-step. In general, α should be chosen slightly larger than the maximum value of

$$\left|\frac{U\,\delta\tau}{\delta X}\right| \text{ or } \left|\frac{V\,\delta\tau}{\delta Y}\right| \text{ or } \left|\frac{W\,\delta\tau}{\delta Z}\right| \text{ occurring in the entire domain.}$$

In other words

$$1 \leq \alpha \leq \text{MAX}\left[\left|\frac{U\,\delta\tau}{\delta X}\right| , \left|\frac{V\,\delta\tau}{\delta Y}\right| , \left|\frac{W\,\delta\tau}{\delta Z}\right|\right] ,$$

An α approximately 1.2 to 1.5 times larger than the right hand number of last inequality is a good choice. Too large an α introduces unnecessary amount of numerical smoothening. (diffusion-like truncation error).

4.5 Software Implementation

The computations have been performed on a HP 9000 (850 series) computer. The computer code consists of several modules. 'DELTAM' is the main program which uses a number of subroutines each of which has a set of specific tasks to carry out.

The given flowchart shows the overall structure of the code with its major communication links between different subroutines and main module. A short description of different indices and the main functions of different subroutines are given below :

IPARA This is an index which indicates whether the calculation

is parabolic (= 1) or elliptic (= 0).

ITYPE This index denotes whether the obstacle is wing (= 1) or winglet (= 2).

IREST This index denotes whether a restart of computing from an existing field variables are desired (= 1) or the computation should start from the very begining (= 0).

INIT This is a subroutine which initializes the entire calculations for a set of input variables such as Reynolds number, Prandtl number, grid sizes etc.

START This subroutine creates the guessed field for the dependent variables and initiates computation.

RESTAR This is a subroutine where the field variables are equated to a data field which was existing beforehand.

ICOPRO This index denotes whether the computation is for constant properties (= 1) or variable properties (= 2).

JSTAM This is a parameter which denotes whether there is stamping on the plates (= 1) or not (= 0)

BCT This is the subroutine for temperature boundary conditions

BCTST This is the subroutine for temperature boundary conditions when there is stamping on the plates.

BCNS This subroutine provides boundary conditions for Navier-Stokes equations.

BCNSST This subroutine provides boundary conditions for Navier-

Stokes equations when there is stamping on the plates.

CONTI This is a main module which solves continuity equation implicitly.

VELALT This is a subroutine which stores the current field variables as the solution for time $\tau = \tau_o$ in order to start a new iteration for time $\tau = \tau_o + \delta\tau$.

TICORR IN this subroutine, the value of time increment $\delta\tau$ and donor cell coefficient α are calculated from stability conditions in each cycle.

OUTPUT This is a subroutine which prints the result files when the preassigned conditions for printing output are met.

ENERGY This subroutine solves the energy equation by an SOR or equivalent technique.

STATE This is the subroutine where the properties are updated through equation of state for variable property solution.NSEQCP In this subroutine velocities for the next time-step are explicitly evaluated through Navier-Stokes equations for constant property calculation.

NSEQVP In this subroutine velocities for the next time-step are explicitly evaluated through Navier-Stokes equations for variable property calculation.

TIGRAD This subroutine calculates the time-gradients of the velocity components.

In the following page, flow chart of the code is given.

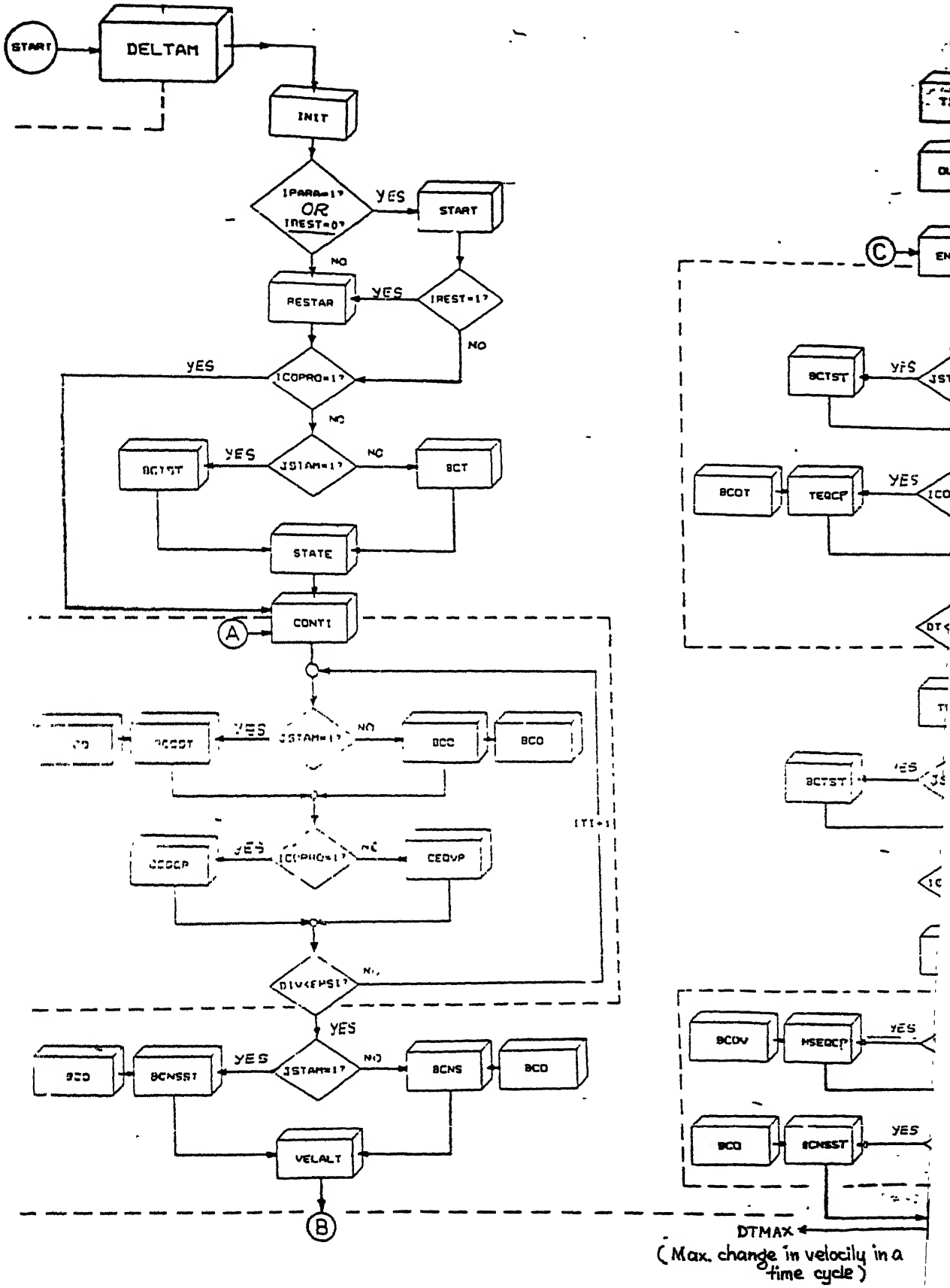
START
DELTAM
INIT
IPARA=1? OR IREST=0?
YES
START
NO
RESTAR
YES
IREST=1?
NO
YES
ICOPRO=1?
NO
BCTST
YES
JSTAM=1?
NO
BCT
STATE
CONT1
A
YES
BCCST
JSTAM=1?
NO
BCO
BCO
YES
CCOCP
ICOPRO=1?
NO
CEOVP
DIV<EPSI?
YES
BCO
BCNSST
YES
JSTAM=1?
NO
BCNS
BCO
VELALT
B
IT1=1
BCTST
YES
BCOT
TEQCP
YES
BCOV
MSEQCP
YES
BCO
BCNSST
YES
DTMAX
(Max. change in velocity in a time cycle)

CHAPTER V

RESULTS AND DISCUSSION

A large number of computations have been performed with delta-wing or a winglet pair as vortex generator under different operating conditions. Subsequently, a comparative performance of wing and winglet has been made through a second-law analysis of the heat transfer process in the channel with the wing or the winglet as the obstacle. Results have been obtained for steady incompressible laminar flow. Air has been taken as the working fluid; hence the Prandtl number of this study is 0.7. Incompressibility assumption is perfectly valid for flow of air in heat exchangers. Laminar flow assumption is also not for computational simplification. Generally, the passage between adjacent plate fins of heat exchangers are so small and the flow velocity is such that the flow is often laminar.

Fig.5 shows the cross-stream velocity vectors at different axial locations in the channel with delta wing as the vortex generator. The position of the chosen cross-sections with respect to the wing has clearly been shown. For slender delta-wing in an infinite medium, leading edge vortices have a vortical structure and they diverge slightly. Now, when we envision a wing moving in an infinite medium, the wake grows longer which, is basically a swirling flow supported by trailing vortices. However the flow in a channel with an attached delta wing shows no trailing edge vortices. Fig.5 shows the generation of vortices and

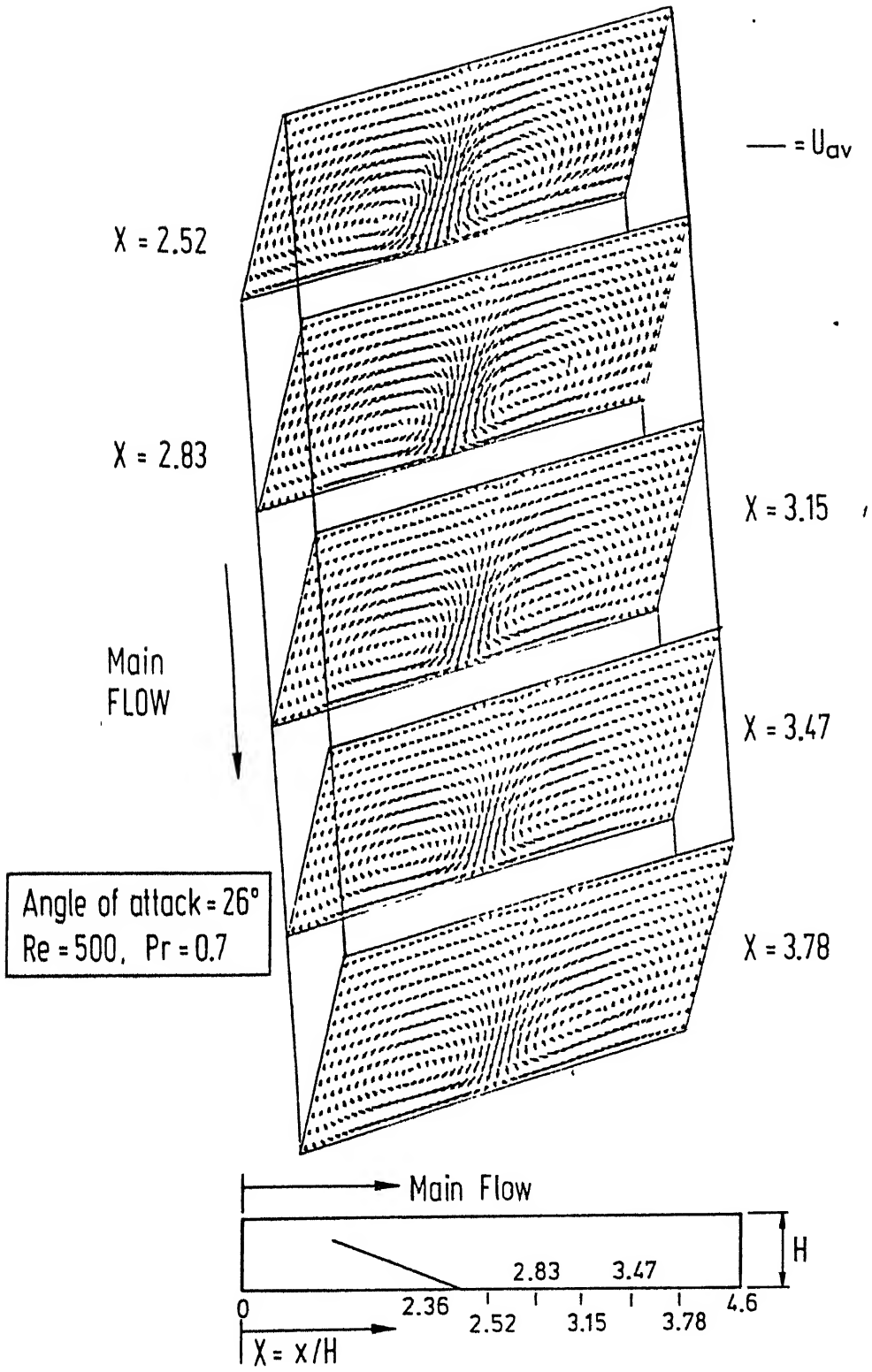

Fig.5 Cross-stream velocity vectors at different axial locations behind the wing showing generation and deformation of vortices in the channel

their elliptic deformation as they move along the channel in presence of a delta-wing. Deformation takes place due to the reduction in strength of the vortices which is brought about by the viscous resistance encountered by the vortical motion in course of its travel.

Fig.6 illustrates the static pressure distribution on two different cross planes in the channel with built-in delta wing. Here we have computed simultaneously developing flow with Reynolds number 1815.The nondimensional static pressure ($p/\rho U_{av}^2$) contours depict that the vortical motion is of free-vortex in nature. Our results follow the same qualitative trends as those observed by Hummel [26] in experiments.

Fig.7 shows the longitudinal velocity vectors along a vertical plane of the channel for the same geometrical and flow parameters as those of Fig.6. For this case of simultaneously developing flow, we have taken uniform velocity profile at the inlet of the channel. The spiralling structure of the flow field due to the presence of the obstacle is evident from this figure.

Fig.8 shows the isotherms at different cross-planes in a channel in presence of a delta winglet pair. The vortex generators influence the temperature field strongly. The spreading of the isotherms over a wider region of the cross-section implies that the bulk temperature is higher in the downstream from the trailing

Re = 1815, Pr = 0.7
β = 20°, Λ = 1.25
α = 3.50

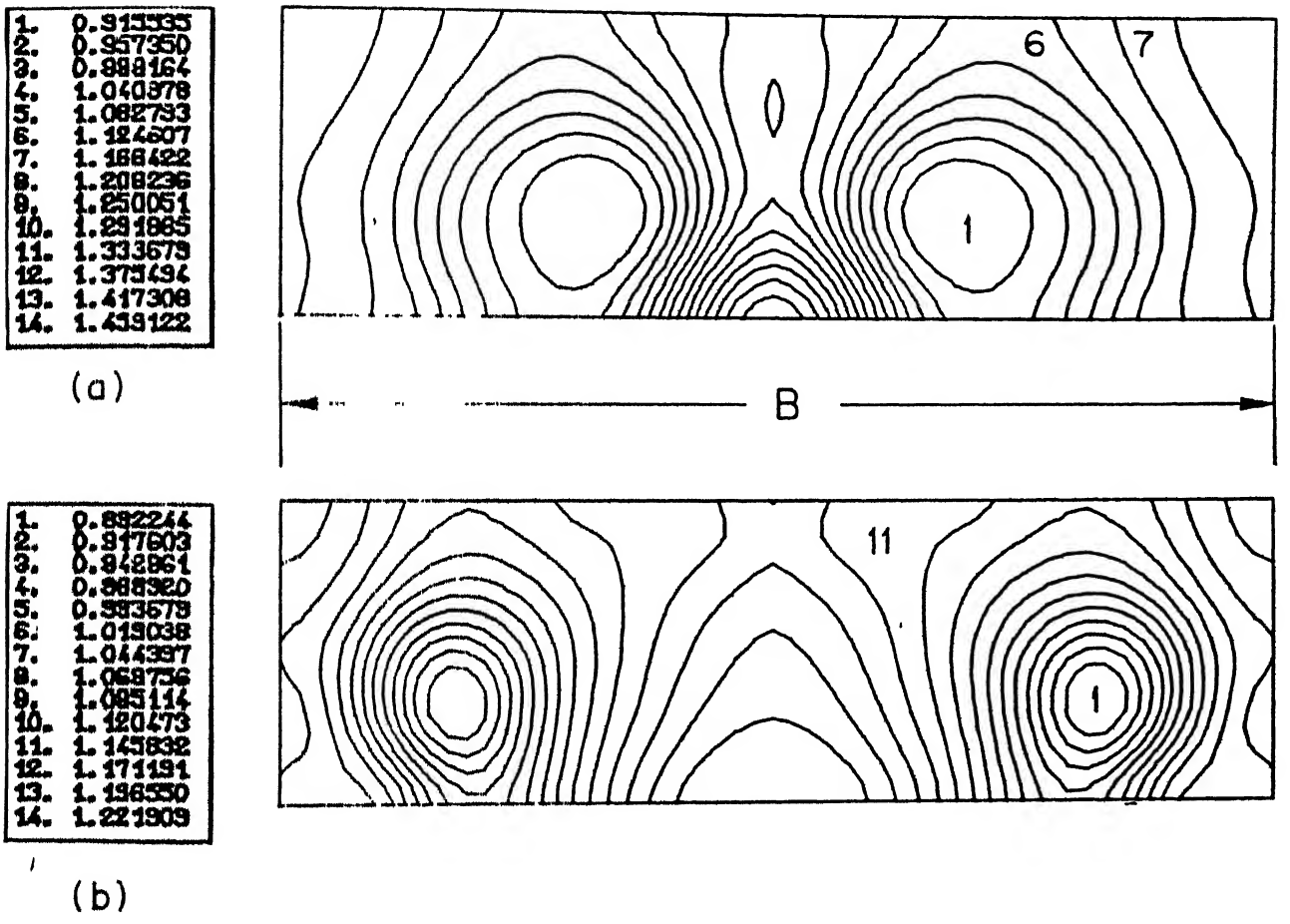

Fig. 6 Distribution of static pressure at two cross-planes: (a) X = 3.5, (b) X = 5.63 from the inlet of the channel

Re = 1815, Pr = 0.7, Λ = 1.25
α = 3.50, β = 20°

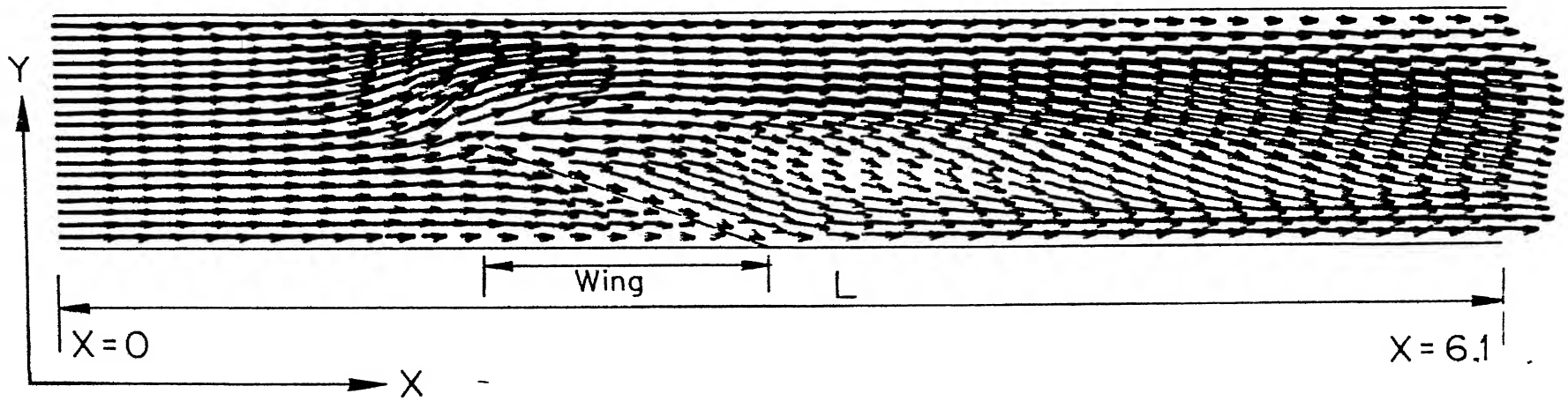

Fig.7 Velocity vectors on a longitudinal section (x-y plane) at a distance Z = 0.625 away from the midplane of the channel.

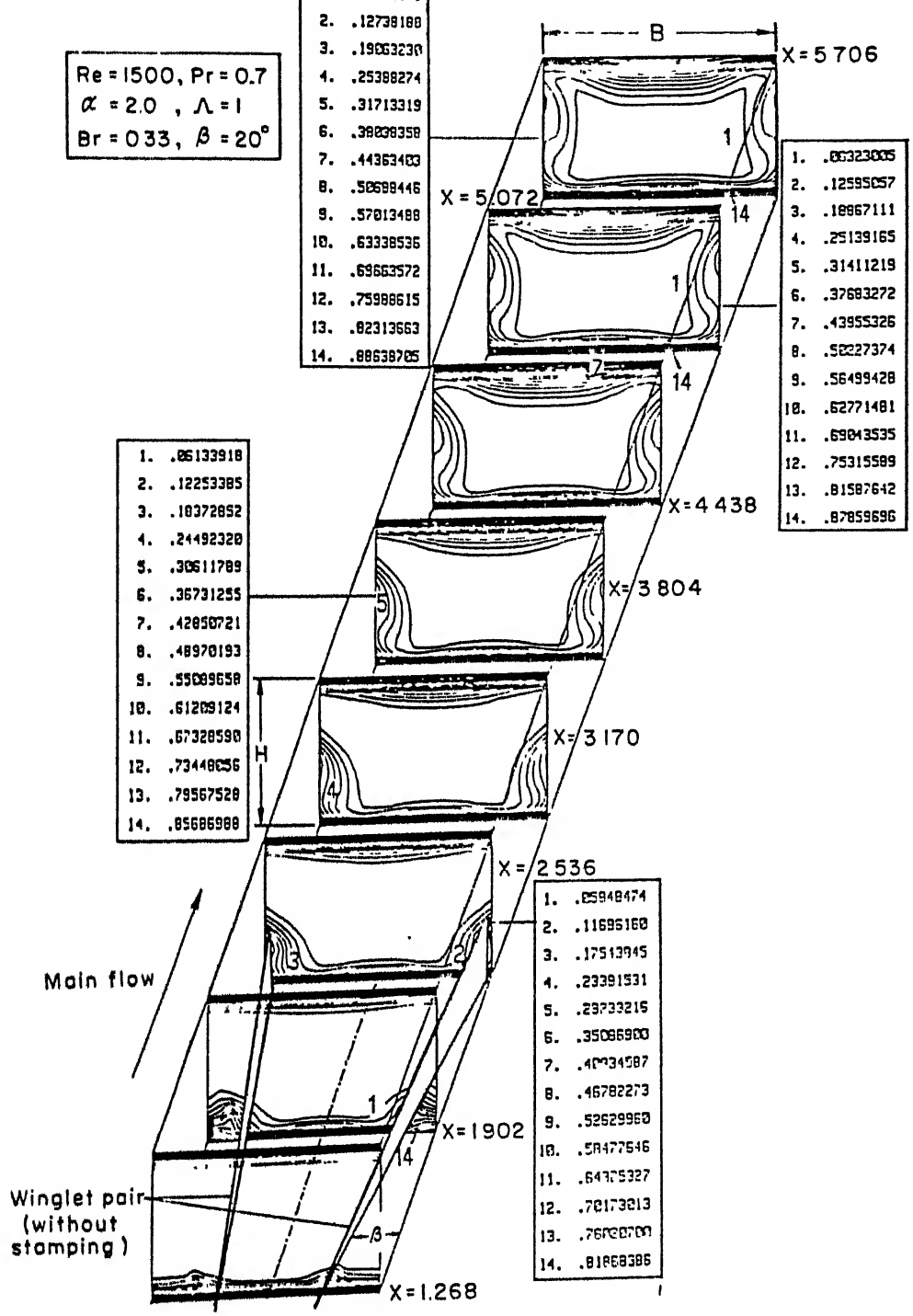

Fig.8 Isotherms at different cross-planes in the channel in presence of a built-in winglet pair

edges of the winglet pair. The importance of the secondary flow and the higher heat transfer is evident from this picture.

As has been stated earlier, we shall also consider the influence of punched holes beneath the wing generators on the heat transfer performance. Fig.9 shows the comparison of cross-stream velocity vectors at different axial locations from the inlet of the channel for the cases without and with stamping on the solid walls. Due to the stamping on the walls a velocity field normal to the vortical motion is induced in the downstream direction. This induced downward normal velocity field reduces the strength of the vortical flow and, as compared with the case where there is no stamping, a decayed circulatory flow pattern is observed at the same axial locations.

Fig.10 shows the heat transfer performance in a channel for a simultaneously developing flow in presence of a delta-wing. The figure also compares the heat transfer for the cases of without and with stamping on the channel walls. In the region of the wing (from X = 2.92 to X = 3.79), the combined spanwise average Nusselt number rises to a high value up to a region behind the middle of the wing and then takes a plunge. A small dead water zone exists in the immediate neighborhood behind the wing-wall junction which causes poor heat transfer at that location. Here, we are referring to the case with built-in delta-wing in the

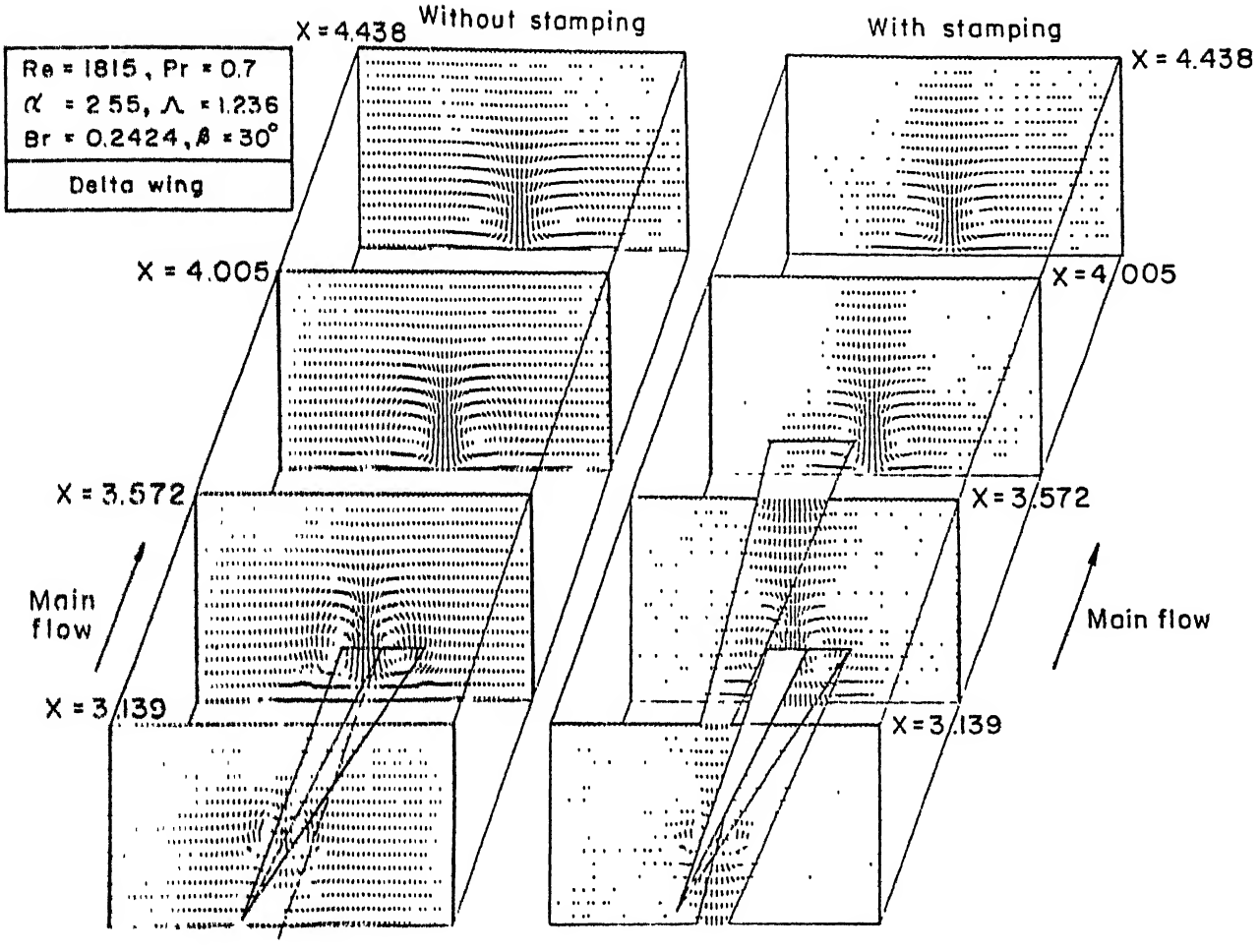

Fig.9. Effect of stamping on cross-stream velocity vectors at different axial locations in the channel with delta wing as the obstacle

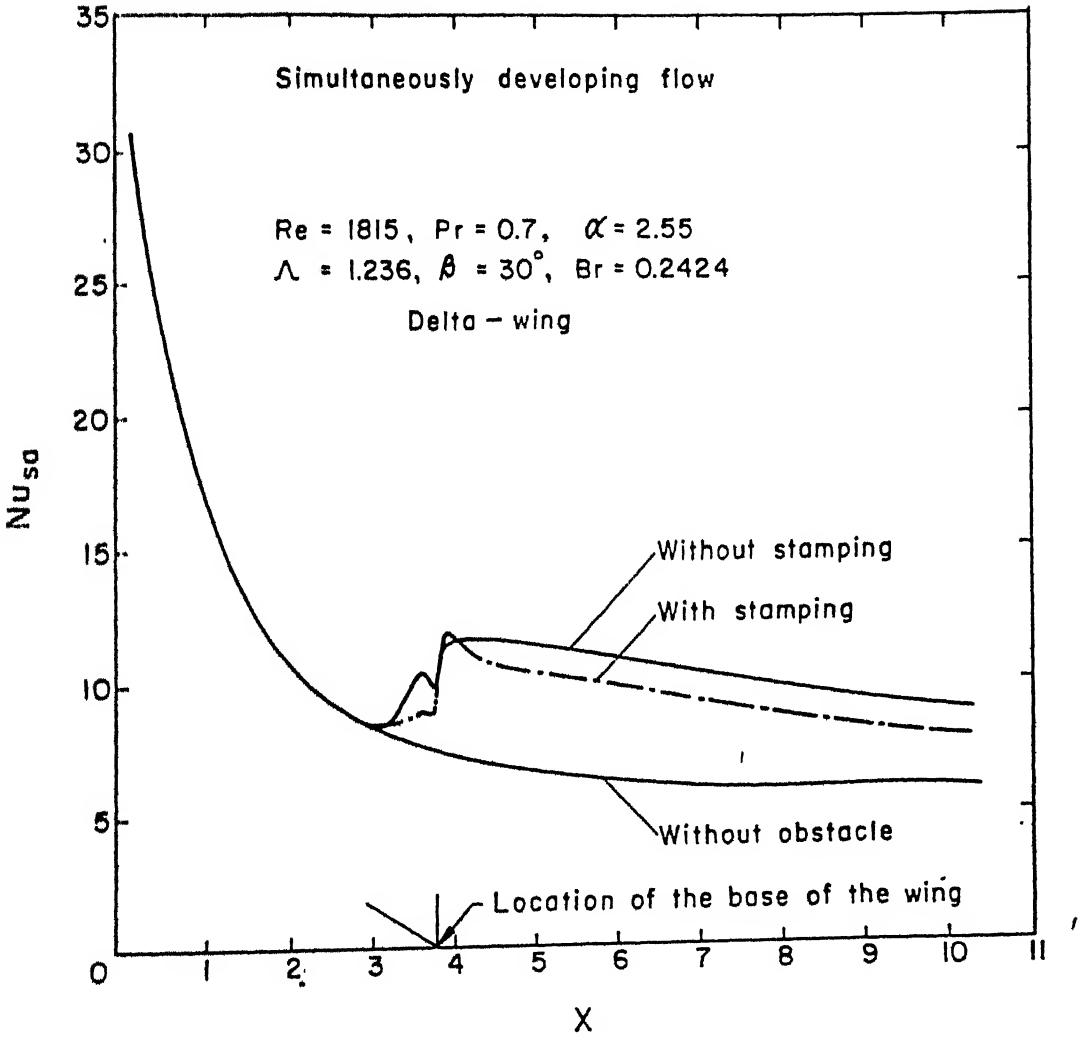

Fig.10 Effect of stamping on the distribution of combined spanwise average Nusselt number in the channel; simultaneously developing flow

absence of any stamping. However, in the downstream of the wing, heat transfer is increased remarkably as compared with the plane channel flow. As such, even for a very long channel (X = 10.28), the enhancement of the heat transfer at the exit of the channel is more than 46.42 percent. Enhancement in heat transfer is not so much when the effect of punched hole beneath the wing is taken into account. Due to the downward normal stream at the cross-planes (as shown in Fig.9), the strength of longitudinal vortices is reduced to a great extent and a spiralling flow with a relatively less vortex strength exists. The improvement in the heat transfer coefficient is relatively lower than that of the case of without any punched hole. However, at the exit of the channel, the improvement of heat transfer as compared with the plane channel is about 29.25 percent. This improvement is indeed better in all other axial locations behind the wing.

Fig.11 shows the influence of angle of attack of the winglet pair on combined spanwise average Nusselt number in the channel. At a nondimensional distance of 4 from the inlet, for an angle of attack of 20°, we observe an enhancement of 30 percent in the combined spanwise average Nusselt number over the case of a channel without any obstacle. Now, at the same location, for an angle of attack of 26°, an improvement of about 6 percent in $\overline{Nu}_{sa}$ over the case of the 20° angle of attack is obtained. However, at

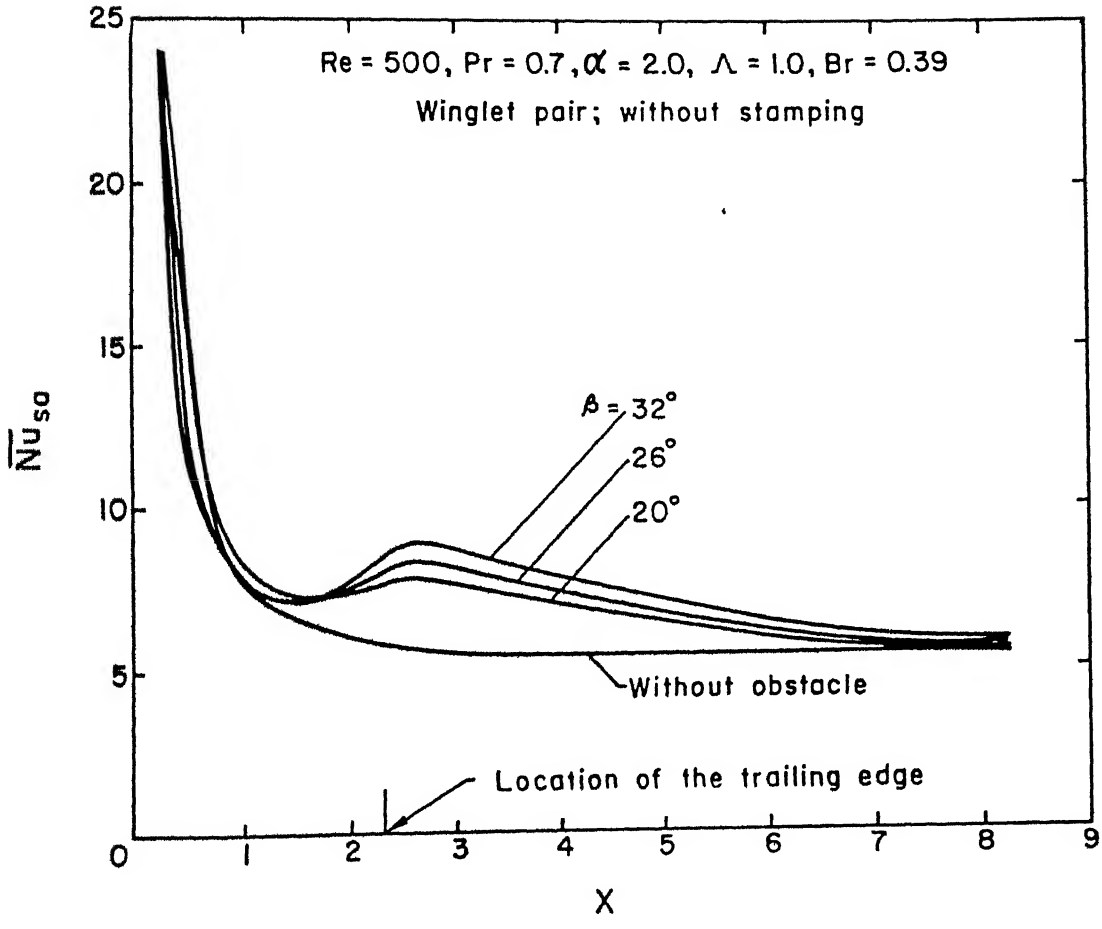

Fig.11 Effect of angle of attack of winglet pair on the distribution of combined spanwise average Nusselt number in the channel

the same location, an improvement of 17 percent over the case of 20° angle of attack is discerned for β = 32°.

Fig.12 compares the relative performance of delta-wing and winglet pair on augmentation of heat transfer. Heat transfer enhancement in the channel behind the vortex generators is clearly evident in both the cases. However, delta wing produces streamwise vortices with higher strength which brings about better improvement in heat transfer as compared with the case of the winglet pair. At a nondimensional distance of 4 from the inlet, the enhancement in combined spanwise average Nusselt number $\overline{Nu}_{ea}$ for a built-in delta wing is more than 31.5 percent than that of a plane channel. The enhancement for the built-in winglet pair at the same location is about 21 percent. It may be mentioned that in case of built-in delta wing, a small dead-water zone exists in the immediate neighborhood behind the wing-body junction which eventually causes poor heat transfer at that location (X = 2.5). The major difference between the wing and the winglet in this application is that the winglet has a free trailing edge whereas, the trailing edge of wing remains attached to the bottom plate. However, in the case of built-in winglet pair, due to the formation of trailing edge vortices, separation bubbles are not formed near the trailing edge and unlike built-in delta wing the zone of poor heat transfer is avoided.

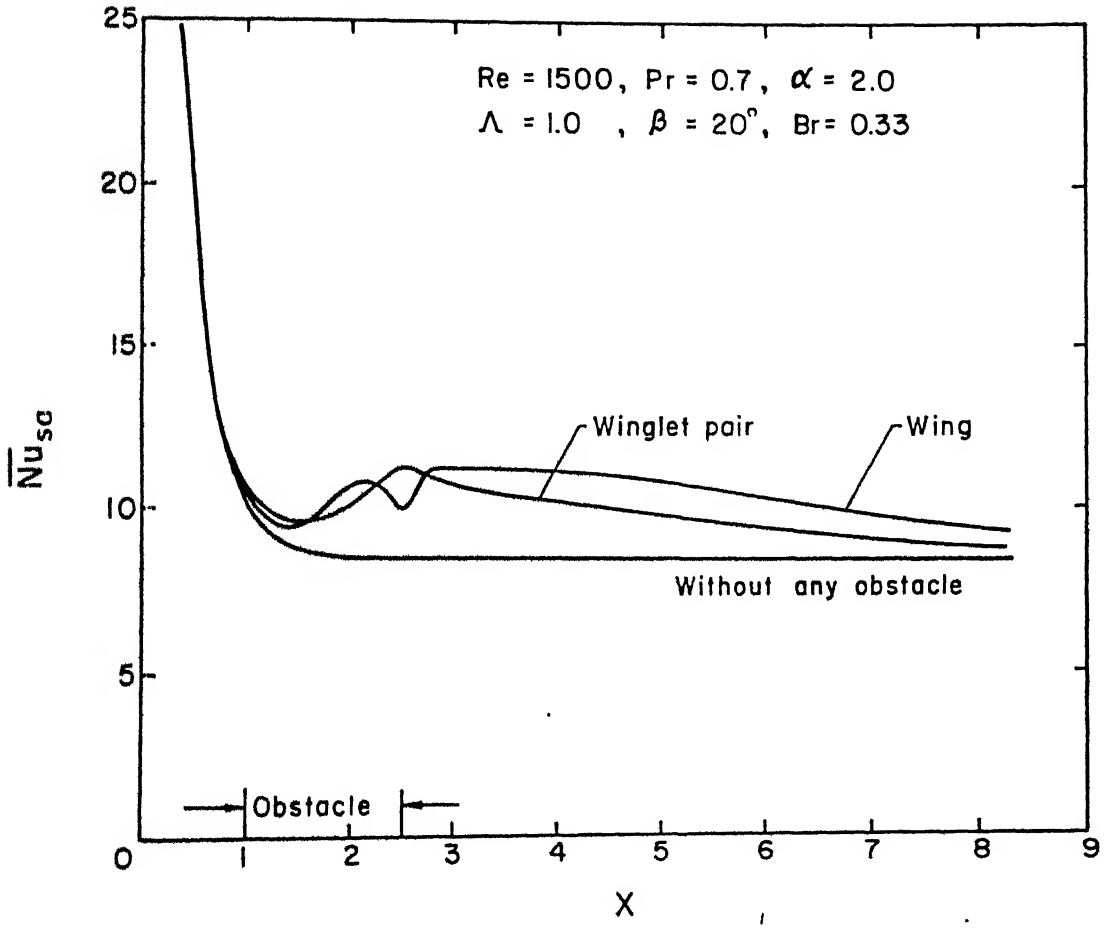

Fig.12 Effect of type of obstacle on the distribution of combined spanwise average Nusselt number in the channel

In order to estimate the flow losses in the channel with built-in vortex generators, the combined spanwise average friction coefficient has been defined as

$$\bar{C}_f = \frac{\mu \left[2 \int_0^{B/2} \left(\frac{\partial u}{\partial y} \right)_{y=0} dz + 2 \int_0^{B/2} \left(\frac{\partial u}{\partial y} \right)_{y=H} dz \right]}{\frac{\rho}{2} U_{av}^2 \, (2 B)} \qquad (29)$$

Fig.13 shows the effect of varying vortex generators (winglet pair) angle of attack on combined spanwise average friction coefficient keeping the size constant. Increasing angle of attack has the effect of increasing vortex strength which increases resistance and consequently, higher value of combined spanwise average friction coefficient is obtained. At the exit of the channel, ($\bar{C}_f \times Re$) for $\beta = 32^\circ$ is 7.49 percent more than that for $\beta = 20^\circ$ and ($\bar{C}_f \times Re$) for $\beta = 26^\circ$ is 3.34 percent more than that for $\beta = 20^\circ$.

Fig.14 compares the distribution of combined spanwise average friction coefficient in a channel for built-in delta wing and winglet pair. As mentioned earlier, delta wing generates streamwise vortices with higher strength and as a consequence, ($\bar{C}_f \times Re$) in a channel is higher for delta wing. At the exit of the channel, ($\bar{C}_f \times Re$) for a delta wing is about 146.6 percent more than that of the channel flow without any obstacle. In the case of built-in winglet pair, the increase in ($\bar{C}_f \times Re$) value

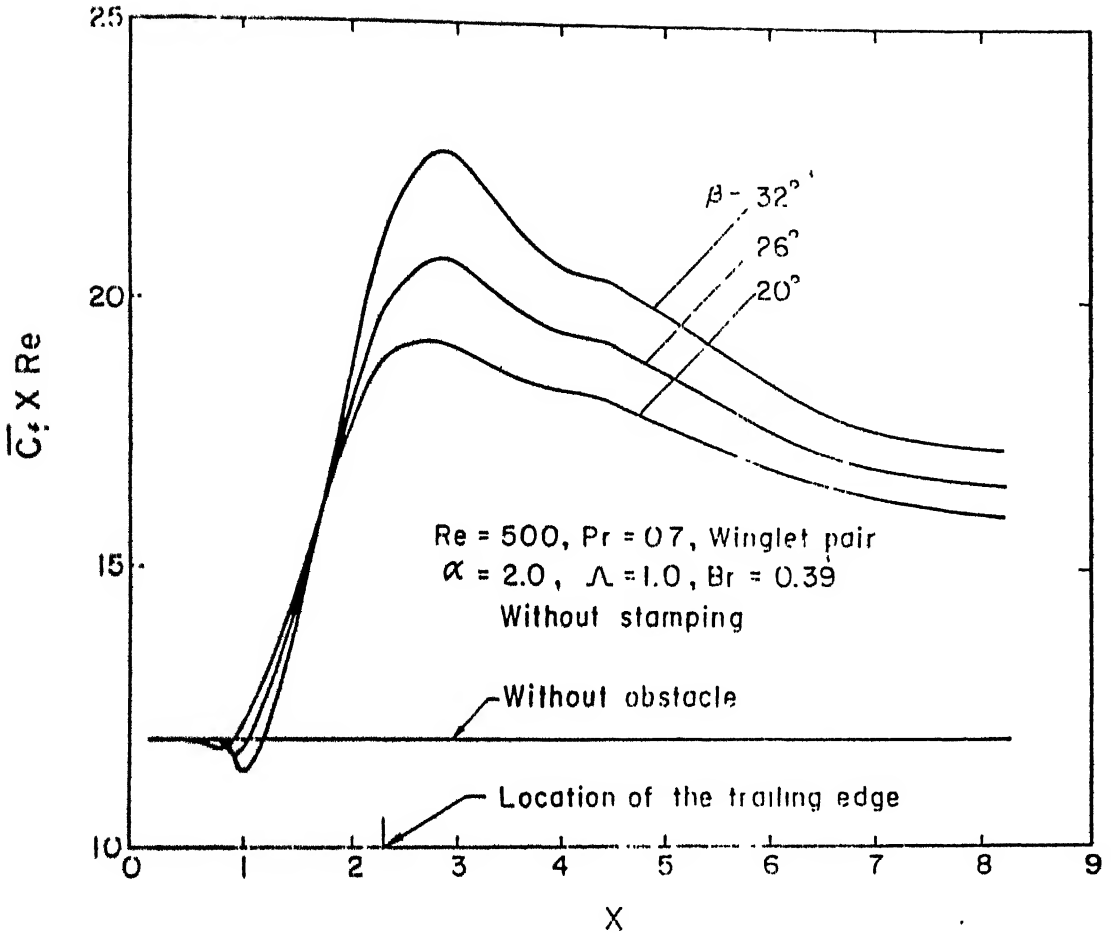

fig.13 Effect of angle of attack of winglet pair on the distribution of combined spanwise average friction coefficient in the channel

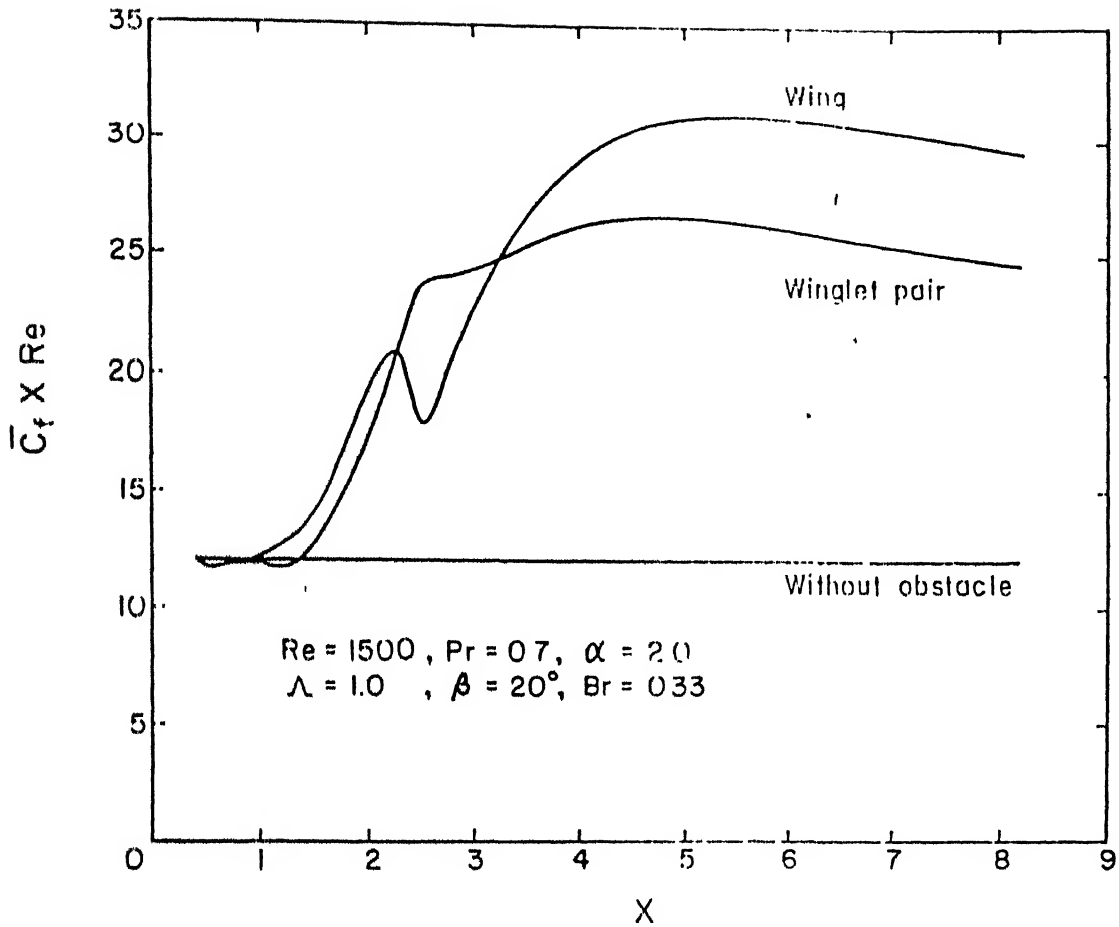

Fig.14 Effect of type of obstacle on the distribution of combined spanwise average friction coefficient in the channel

at the same location over the ($\bar{C}_f \times Re$) of a plane channel is nearly 100 percent. It may be mentioned that the Reynolds number for this computation is 1500.

Fig.15 shows the variation of merit function, M with Reynolds number (in the range of 500 - 3000) for the built-in delta winglet pair. This figure shows that the delta winglet pair displays better performance than delta wing with regard to merit function. With increasing Reynolds number, the delta wing generates vortices with higher strength which culminates in steeper velocity gradients compared to the winglet pair. As a result, frictional losses become high and consequently, the total entropy generation becomes much more pronounced for built-in delta wing. For the case of heat transfer in a channel with built-in winglet pair, the increase in irreversibility associated with the increase in exergy transfer occurs at a relatively lower rate as compared to the case with a built-in delta wing. From the view point of second-law efficiency, the use of built-in winglet pair has edge over the built-in delta wing. Although with regard to augmentation of heat transfer in the channel, the built-in delta wing shows better performance, it can be certainly argued that the built-in winglet pair is more effective with respect to energy transferred usefully.

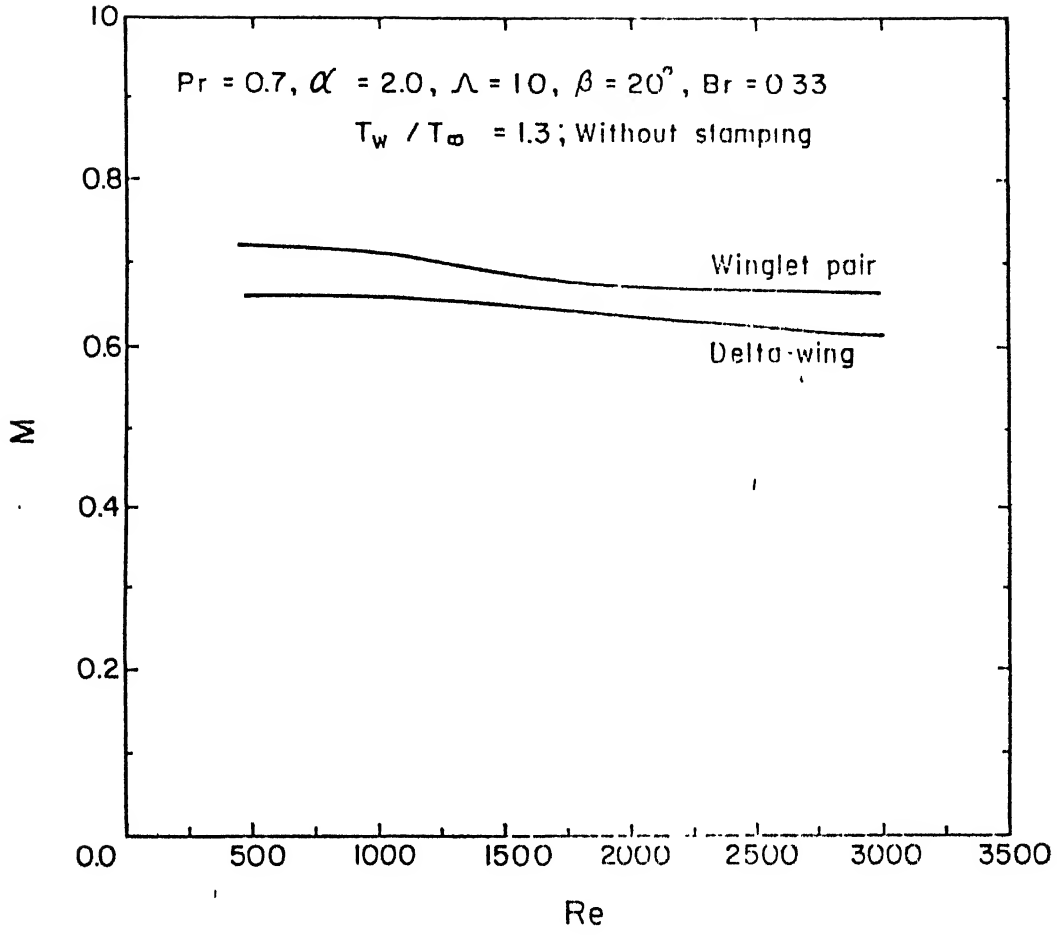

Fig.15 Effect of type of obstacle on the variation of merit function with Reynolds number

Because of non-availability of experimental data-base, the model validation was not accomplished extensively. However, one more comparison with respect to mean-Colburn-factor enhancement (Δj) using delta wing for two different angles of attack was performed. The experimental results were obtained from Kallweit (1986). In the experiment, the reference plate-fin area started from the location of the base of the wing; its longitudinal extent was 7.5 wing lengths and its lateral extent was 4 times the wing span. Identifying this zone on the bottom plate as the reference area, experiments were conducted in a plane channel and in a channel with built-in delta wing at different angles of attack. Experimentally obtained mean-Colburn-factor enhancements (Δj) over the reference area due to the delta wing with angles of attack 20° and 30° are 1.1×10^{-3} and 1.425×10^{-3} respectively. Reynolds number for this experiment is 1815 and air is used as the flowing fluid (Pr=0.7). Computations were performed in similar geometrical configurations by making use of our model (and hybrid scheme of discretization) and the corresponding mean-Colburn-factor enhancement values (Δj) were found to be 1.0178×10^{-3} and 1.7×10^{-3} for the angles of attack of 20° and 30° respectively. The numerical model and the experiment corroborate each other reasonably.

CHAPTER VI

CONCLUDING REMARKS

Irreversibility, quantified by the rate of entropy generation , plays a significant role in convective heat transfer processes. The second-law analysis seeks to evaluate the rate of entropy generation in various processes and thereby, select the process which has minimum entropy generation rate and hence is, thermodynamically, the most viable one. It has already been observed that significant improvements may be brought about in heat exchanger design by making use of wing-type vortex generators on the plate-fins. However, based on a comparative study of second-law efficiency, use of winglets appears to be a more effective augmentation technique.

REFERENCES

1. Edwards, F. J. and Alker, G. J. R., 1974, The Improvement of Forced Convection Surface Heat Transfer Using Surface Protrusions in the Form of (a) Cubes and (b) vortex generators, Proceedings of the Fifth Int. Heat Transfer Conference, Tokyo, Vol. 2, pp 2244 -2248.

2. Russel, C. M. B., Jones, T. B. and Lee, G. H., 1982, Heat Transfer Enhancement Using Vortex Generators, Proceedings of The Seventh Int. Heat Transfer Conference, Munich, Vol. 3, pp 283 - 288.

3. Fiebig, M., Kallweit, P. and Mitra, N. K., 1986, Wing Type Vortex Generators for Heat Transfer Enhancement, Proceedings of the Eighth Int. Heat Transfer Conference, San Francisco, Vol. 6, pp 2909 - 2913.

4. Fiebig, M., Brockmeier, U., Mitra, N. K. and Güntermann, T., 1989, Structure of Velocity and Temperature Fields in Laminar Channel Flows with Longitudinal Vortex Generators, Numerical Heat Transfer, Vol. 15, pp 281 - 302.

5. Biswas, G., Mitra, N. K. and Fiebig, M., 1989, Computation of Laminar Mixed Convection Flow in a Channel with Wing Type Built-In Obstacles, Journal of Thermophysics and Heat Transfer (AIAA), Vol. 3, pp 447 - 453.

6. Eibeck, P. A. and Eaton, J. K., 1987, Heat Transfer Effects of a Longitudinal Vortex Embedded in a Turbulent Shear Flow, Journal of Heat Transfer, Vol. 109, pp 16 - 24.

7. Ligrani, P. M., Subramanian, C. S., Craig, D. W. and Kaisuwan, P., 1991, Effects of Vortices with Different Circulations on Heat Transfer and Inertant Downstream of a Row of Film Cooling Holes in a Turbulent Boundary Layer, Journal of Heat Transfer, Vol. 113, pp 79 - 90.

8. Biswas, G. and Chattopadhyay, H., 1991, Heat Transfer In A Channel with Built-In Wing-Type Vortex Generators, International Journal of Heat and Mass Transfer (to appear).

9. Fiebig, M., Kallweit, P., Mitra, N. K. and Tiggelbeck, S., 1991, Heat Transfer Enhancement and Drag by Longitudinal Vortex Generators in Channel Flow, Experimental Thermal and Fluid Science, Vol. 4, pp 103 - 114.

10. van Dyke, M., 1982, An Album of Fluid Motion, Published by the Department of Mechanical Engineering, Stanford University, California, USA.

11. Winter, H., 1956, Strömungsvorgänge on Plattern and Profilerten Körpern bei Kleinen Spannweiten, Forschg. Ing. Wes., Vol. 6, pp 247 - 249.

12. Fink, P. T., 1956, Wind-Tunnel Tests on a Slender Delta Wing at High Incidence, Z. Flugwiss, Vol. 4, pp 247 - 249.

13. Mardsen, D. J., Simpson, R. W. and Rainbird, W. J., 1958, The Flow over Delta Wing at Low Speeds with Leading Edge Separation, College of Aeronautics, Cranfield, Rep. 114.

14. Peckham, D. H., 1958, Low Speed Wind Tunnel Experiments on Series of Sharp-Edged Delta Wings, RAE Rep. Aero 2613.

15. Earnshaw, P. B. and Lawford, J. B., 1961,Low Speed Wind Tunnel Experiments on Series of Sharp Edged Delta Wings, Part 1,RAE TN Aero 2780.

16. Lawford, J. A., 1964, Low Speed Wind Tunnel Experiments on Series of Sharp-Edged Delta Wings, Part 2,RAE Rep. Aero 2954.

17. Bollay, W., 1939, A Nonlinear Wing Theory and Its Application to Rectangular Wings at Small Aspect Ratio, ZAMM, Vol. 19, pp 21 - 35.

18. Brown, C. E. and Michael, W. H., 1954, Effect of Leading Edge Separation on the Lift of a Delta Wing, J. Aero Sci., Vol. 21, pp 690 - 694.

19. Mangler, K. W. and Smith, J. H. B.,1959, A Theory of Flow Past a Slender Delta Wing with Leading Edge Separation, Proc. Roy. Soc. Lond., A251, pp 200 - 217.

20. Smith, J. H. B., 1968, Improved Calculations of Leading Edge Separation from Slender Delta Wings. Proc. Roy. Soc. Lond., A306, pp 67-90.

21. Rehbach, C., 1976, Numerical Investigations of Leading-Edge

Vortex for Low Aspect-Ratio Thin Wings, AIAA J., Vol. 14, pp 253 - 255.

22. Kandil, O. A., Mook, D. T. and Nayfeh, J. H., 1976, Nonlinear Prediction of Aerodynamic Loads on the Lifting Surfaces, J. Aircraft, Vol. 13, pp 22 - 28.

23. Johnson, F. T., Lu, P., Brune, G. W., Webber, J. A. and Rubbert, P. E., 1976, An Improved Method for Prediction of Complete Three Dimensional Aerodynamic Load Distribution on Configurations with Leading-Edge Separation, AIAA paper no. 76 - 147.

24. Johnson, F. T., Lu, P., Brune, G. W., Webber, J. A. and Rubbert, P. E., 1976, Application of a Higher Order Subsonic Panel Method to Configuration with Free Vortex Flow, EUROMECH Colloqu., 75, Rhode (Braunschweig).

25. Hummel, D. and Srinivasan, P. S., 1967, Vortex Breakdown Effects on the Low-Speed Aerodynamic Characteristics of Slender Delta Wings in Symmetrical Flow, J. Roy. Aero. Soc., Vol.71, pp 319 -322.

26. Westphal, R. V. and Mehta, R. D., 1987, Interaction of an Oscillating Vortex with a Turbulent Boundary Layer, AIAA 19th Fluid Dynamics and Laser Conference, Hawaii, AIAA paper no. 87 - 1246.

27. Brockmier, U., Mitra, N. K. and Fiebig, M., 1987, Navier-

Stokes Computation of Three Dimensional Laminar flow Fields in a Channel with Wing Type Vortex Generators, Proc. of Second International Symposium on Computational Fluid Dynamics, Sydney.

28. Achaichia, A. and Cowell, T. W., 1988, Heat Transfer And Pressure Drop Characteristics Of Flat Tube And Louvered Plate Fin Surfaces, Experimental Thermal And Fluid Science, Vol. 1, pp 147 - 157.

29. Bejan, A., 1977, The Concept of Irreversibility in Heat Exchanger Design, ASME Journal of Heat Transfer, Vol. 99, pp 374 -380.

30. Bejan, A., 1978, General Criterion for Rating Heat Exchahger Performance, International Journal of Heat and Mass Transfer, Vol. 21, pp 655 - 658.

31. Bejan, A., 1979, A Study of Entropy Generation in Fundamental Convective Heat Transfer, ASME Journal of Heat Transfer, Vol. 101, pp 718 - 725.

32. Bejan, A. and Smith, J. L., Jr., 1975, Heat Exchangers for Vapour Cooled Conducting Supports of Cryostats, Adv. Cryog., Engg., Vol. 21, pp 247 -256.

33. Sarangi, S. and Chowdhury, K., 1982, On the Generation of

Journal of Computational Physics, Vol. 10, pp 324 - 340.

41. Chorin, A. J., 1967, A Numerical Method for Solving Incompressible Viscous Flow Problems, J. Comp. Physics, Vol. 2, pp 12 - 26.

42. Viecelli, J. A., 1971, A Computing Method for Incompressible Flows Bounded by Moving Walls, Journal of Computational Physics , Vol. 8, pp 119 - 143.

43. Spalding, D. B., 1972, A Novel Finite Difference Formulation for Differential Expressions Involving Both First and Second Derivatives, Int. J. Numer. Methods in Engineering, Vol. 4, pp 551 - 559.

44. Pyret, R. and Taylor, T. D., 1975, Computational Methods for Fluid Flows, Los Alamos Scientific Lab., Rep. LA - 5642.

45. Brandt, A., Dendy, J. E. and Ruppel, H., 1980, The Multigrid Methods for Semi-Implicit Hydrodynamic Codes, J. Compu. Phys., Vol. 10, pp 348 - 370.